CHAPTER 6

N92-15458

Trends in Stratospheric Temperature

Panel Members

M. R. Schoeberl, Chapter Chair
P. A. Newman, Observations Subgroup Chair
J. E. Rosenfield, Modeling Subgroup Chair

J. Angell   A. J. Miller
J. Barnett   J. Nash
B. Boville NH 315709   V. Ramaswamy
S. Chandra   F. Schmidlin
S. Fels   M. Schwarzkopf
E. Fleming   K. Shine
M. Gelman
K. Labitzke F 7115851

Chapter 6

Trends in Stratospheric Temperature

Contents

6.1 INTRODUCTION

The purpose of this chapter is to examine stratospheric temperatures for long-term and recent trends, discuss the mechanisms that can produce atmospheric temperature trends, and determine if observed changes in upper stratospheric temperatures are consistent with observed ozone changes.

The long-term temperature trends are determined up to 30 mb from radiosonde analysis (since 1970) and rocketsondes (since 1969 and 1973) up to the lower mesosphere principally in the Northern Hemisphere. The more recent trends (since 1979) incorporate satellite observations.

Previously published stratospheric temperature trend analyses used a variety of statistical techniques and data bases; as a result, intercomparison has been difficult. Here, data sets from the Free University of Berlin, the U.S. National Meteorological Center (NMC) of the National Oceanic and Atmospheric Administration (NOAA), the United Kingdom Meteorological Office (UKMO), and radiosonde and selected rocketsonde information are compared. The data set descriptions, intercomparisons, and trends make up Sections 6.2 and 6.3 of this report.

In Section 6.4, the mechanisms that can produce recent temperature trends in the stratosphere are discussed. The following general effects have been considered: changes in ozone, changes in other radiatively active trace gases, changes in aerosols, changes in solar flux, and dynamical changes. Radiative equilibrium experiments have been performed with carefully calibrated radiative transfer codes to quantify the magnitude of the temperature changes expected with ozone and solar flux changes. In particular, computations have been made to estimate the temperature changes associated with the upper stratospheric ozone changes reported by the SBUV instrument aboard Nimbus-7 and the SAGE instruments. The conclusions of this report are given in Section 6.5.

6.2 TEMPERATURE DATA SET DESCRIPTION

6.2.1 Radiosonde

6.2.1.1 Introduction

Radiosondes continue to provide the basic upper air data for meteorological services. The users are a diverse group, including meteorologists who are involved in operational numerical weather analysis and forecasting, and climatologists who are interested in the long-term variations of quantities such as temperature. The accuracy of the temperature, pressure, and humidity measurements obtained from radiosondes is particularly important to these users. However, the accuracy required for day-to-day operations is not the same as that required for the study of long-term trends; understandably, it is the accuracy required by the former that has received the most attention.

6.2.1.2 Radiosonde Errors

Specification of the errors of the various radiosonde systems in regular worldwide use has proven difficult. A relatively inexpensive "standard" instrument for calibration purposes has never been developed; in the absence of a reference instrument, different methods have been used in an attempt to judge the quality of radiosonde instruments, including the evaluation of

447

day–night differences in observational reports. A very useful method of comparing the measurement capabilities of radiosondes is instrumental intercomparison, whereby multiple radiosondes are carried aloft on a single balloon.

The most recent, and largest ever, series of radiosonde intercomparisons, organized by the WMO Commission on Instrument and Method of Observation (CIMO), was carried out at Bracknell, England, in 1984, and at Wallops Island, Virginia, USA, in 1985 (Nash and Schmidlin, 1987). The main findings, based on eight radiosonde types used in the intercomparisons, are:

- The reproducibility of temperature measurements was about 0.2K in most cases.

- The reproducibility of pressure measurements varied from 0.5 to about 2.0 mb.

- Different radiosonde instruments showed different time constants of response, which can lead to appreciable difference in temperature estimates at given levels.

- Performance of the pressure sensor can be critical to temperature estimates at heights above 20 mb (assignment of the temperature to an incorrect pressure level).

As an example of these problems, Figure 6.1 displays a plot of consistent temperature differences for a variety of radiosonde instruments (reprinted from Nash and Schmidlin, 1987). Above the 50 mb level, instrument differences can be larger than 1K. The number of different types of radiosonde in use at any time is not small (~17). Thus, the continuity and accuracy of long-term trends are also subject to errors caused by modifications in design, manufacture, and data reduction.

These findings have an obvious impact on operational analyses, in which accuracy is important, but their impact on trend analysis, in which precision is most important, may not be as great. What is important in trend measurement is that the observations at individual stations be consistent in time; in the attempt to improve accuracy based on the above findings, it is this consistency that is lost. It is not clear that the operational radiosonde network now in place will ever prove entirely satisfactory for the detection of long-term variations in quantities such as temperature. Nevertheless, radiosondes provide, and probably will continue to provide, the primary data set for long-term lower stratospheric temperature trend assessment.

6.2.1.3 Description of the Radiosonde Data Sets

Two radiosonde-based data series are readily available for the investigation of long-term temperature and geopotential height changes in the lower stratosphere, such as 30 mb. The Northern Hemisphere daily analyses, carried out by the Stratospheric Research Group of the Free University of Berlin, are based mainly on radiosonde observations at 00 and 12 UT (about 900 observations per day). Since 1980, these analyses have included satellite data taken over the oceans (Labitzke et al., 1985). Because these analyses are a research project, carried out only after all data have been received, consistency in time is achieved. The daily charts are digitized on a 10 by 10 latitude–longitude grid, and monthly zonal-mean temperatures are obtained. Over the middle latitudes, each monthly zonal mean value of temperature is based on approximately 3,000 observations, resulting in a extremely small sampling error. Another advantage of this technique is that errors of single stations on single days can be eliminated by comparison with other stations nearby, and missing data can be interpolated. This data set starts in July 1964 for most stratospheric pressure surfaces.
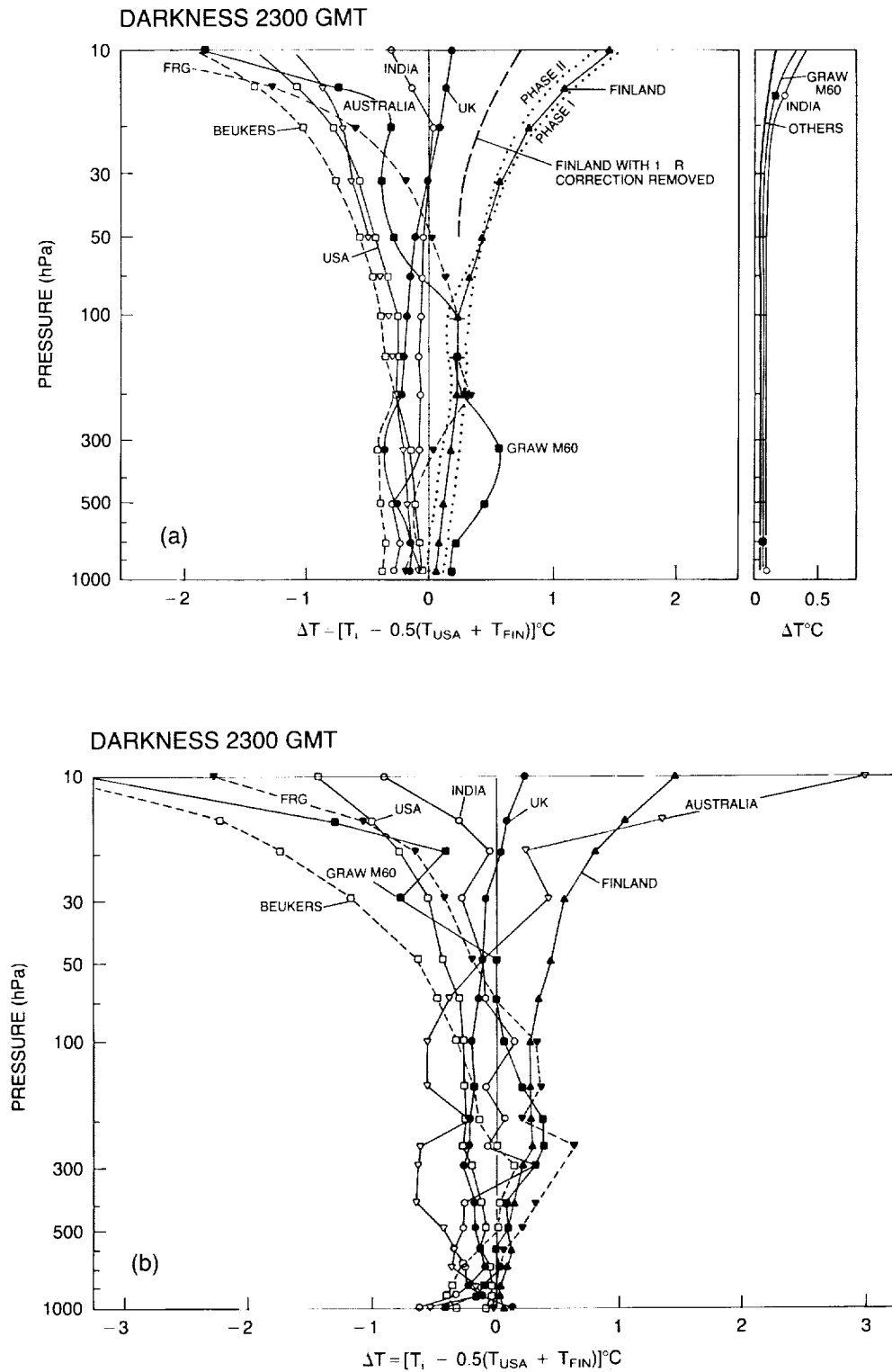
Figure 6.1 Intercomparison of different radiosondes at night (from Nash and Schmidlin, 1987). T_i is the temperature measured by the particular instrument. (a) Temperature differences from a standard defined by the U.S. and Finnish instruments. (b) As in (a), but reported on standard pressure surfaces. Note the increased error caused by the information in the pressure sensor.

The second temperature series, from Angell and Korshover (1983a), is based on the variation of height difference or thickness (proportional to mean temperature) between 100 and 30 mb at 63 radiosonde stations distributed worldwide, 45 of which are in the Northern Hemisphere. At each station for each year, the seasonal deviation of thickness from the long-term seasonal mean has been determined; these station deviations have then been averaged for polar, temperate, subtropical, and equatorial zones, as well as for both hemispheres and the world, by the use of area weighting. This data set generally begins in 1958, but because Soviet Union radiosonde data were not available before 1970, the temperature variations in north polar and north temperate climatic zones are not represented before that date. Because of the relatively small number of radiosonde stations used in this analysis, this technique is much more sensitive to erroneous station data or missing data than is the previous technique. The two data sets are intercompared in Section 6.3.1.

6.2.2 Satellite

6.2.2.1 Introduction

Before 1978, several satellite temperature sounders were in use with weighting functions in the stratosphere and mesosphere, including the Vertical Temperature Profile Radiometer (VTPR), the Selective Chopper Radiometer (SCR), and the Pressure Modulated Radiometer (PMR). Data from these have not been used for trend analysis because the available data are not of sufficient accuracy or record length. For example, the PMR data for the upper stratosphere and mesosphere would have been of particular interest but, although the instrument appeared to be stable, the data record extended only for 3 years.

The TIROS–N Operational Vertical Sounder (TOVS) Series began operation in late 1978. TOVS comprises three radiometers that provide observations of narrow bandwidth radiance, originating primarily from the stratosphere and troposphere. The radiometers are the High-resolution Infrared Sounder (HIRS–2), the Stratospheric Sounding Unit (SSU), and the Micro-wave Sounding Unit (MSU); their nominal performance is outlined in Smith et al. (1979). These instruments measure the thermal emission from layers of the atmosphere, as indicated by the weighting functions given in Figure 6.2a. The present series of the TIROS–N spacecraft is expected to remain in operation beyond 1990; hence, the current type of sounders has the potential to provide a monitor of stratosphere temperature trends over at least 10 years. However, because not all of the spacecraft will carry the principal stratosphere sounder, the SSU, the quality of trend information can be expected to diminish during the rest of the decade.

These emitted radiances from Earth's atmosphere may be individually converted to an equivalent temperature for each layer (known as the brightness temperature) or may be retrieved to obtain a temperature profile or layer mean temperature between fixed pressure levels. It should be noted that the measurements are obtained on a vertical pressure scale (as opposed to height).

Two methods for determining stratospheric temperature changes from the TOVS data will be discussed. Nash and Forrester (1986) used the zonal mean measurements from several radiometer channels. Their work was aimed primarily at trend-type studies, without performing any temperature retrieval. They established reproducibility and systematic drifts in both the radiometric (i.e., temperature) and the spectroscopic (i.e., weighting function) performance by careful comparison between different sounders in simultaneous operation and by careful prelaunch calibration. Estimates of temperature trends since late 1979 were derived for layers of
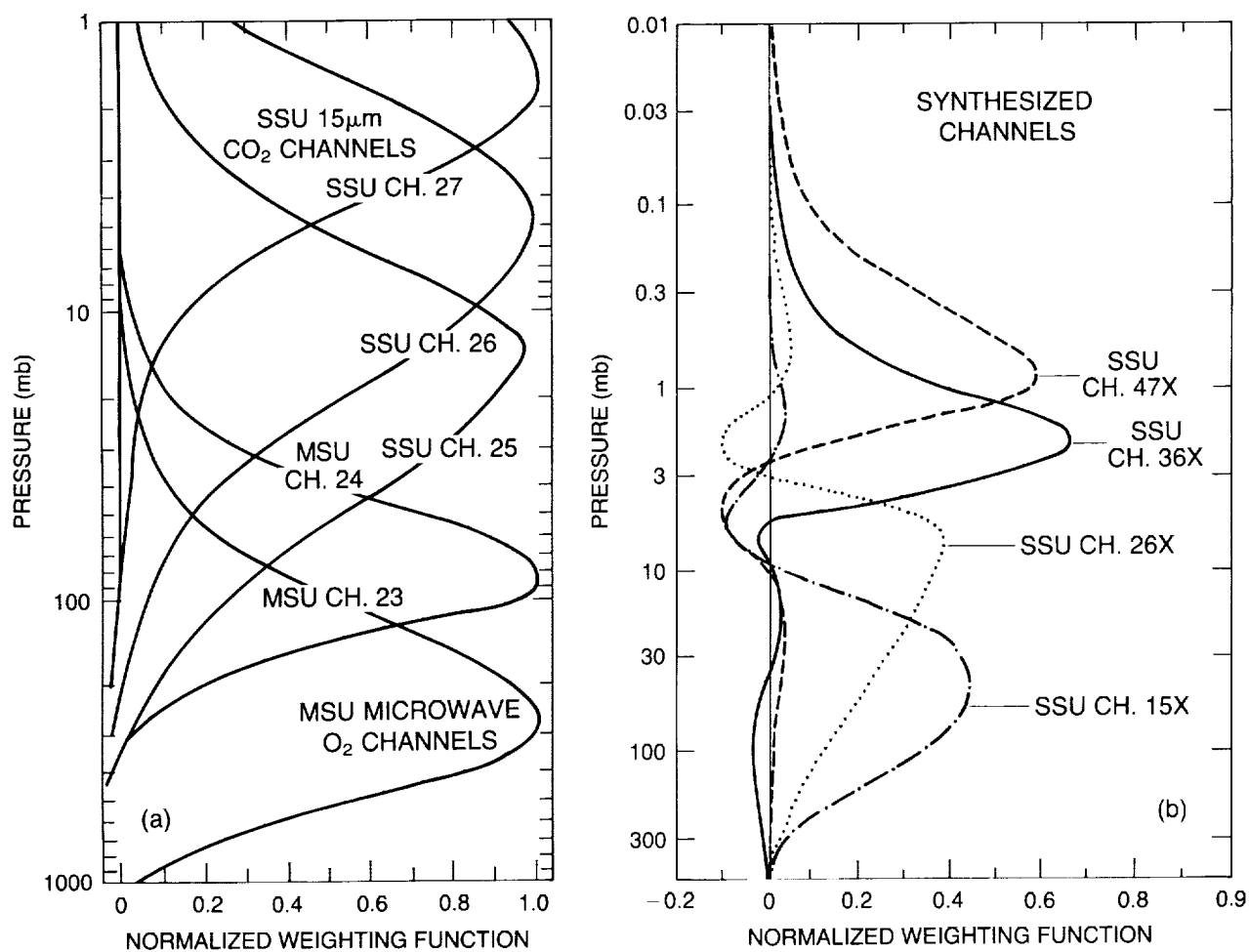
Figure 6.2 Weighting functions for satellite temperature instruments: (a) MSU, SSU; (b) Synthesized SSU channels from Nash (1987).

the atmosphere centered at pressures between 90 and 0.5 mb. Their method is discussed in detail in Section 6.2.2.2.

Gelman et al. (1986) use global stratospheric temperature fields derived as an operational product from the National Meteorological Center. In contrast to the Nash and Forrester method, a temperature retrieval process is used first to give temperatures as a function of latitude, longitude, and pressure. Because data from only one satellite are used at any one time, periods of overlap are not available for intercomparison. The fields were retrospectively adjusted (primarily using comparisons with rocketsonde data) to compensate for differences between the successive satellites in the TIROS–N series. This data set is discussed in Section 6.2.2.3.

6.2.2.2 Radiance Data

NOAA spacecraft have been in simultaneous operation for most of the time since late 1978. Comparison of observations obtained by the nominally identical TIROS Operational Vertical Sounders (TOVS) from two simultaneously operated spacecraft in the TIROS–N/NOAA series has allowed a check on the stability of their radiometer performance.

The comparison data used in this report were previously described by Nash and Forrester (1986) and were obtained by an extension of the methods used in earlier studies of SSU performance by Pick and Brownscombe (1981) and Nash and Brownscombe (1983).

The TOVS channels chosen for analysis have been limited to those with relatively high vertical resolution (i.e., 10 to 15 km), namely MSU and SSU. The stratospheric HIRS–2 channels have poor vertical resolution and contribute only redundant information. Processed radiance observations from these channels have been separated according to radiometer view angle and used to generate zonally averaged mean radiances for 10 latitude bands centered from 70°N to 70°S for each day. Radiances from the nadir or near-nadir views have been used in each case. Further independent information is obtained through a procedure described by Nash (1988) in which differences are taken between the zonal mean SSU radiances at 35° and 5° to nadir. The 35° weighting functions are at higher altitudes (because of limb effects), and combinations can be found that are either sharper than the contributing weighting functions or at higher altitudes. This technique provides the highest altitude weighting function, known as 47X, which is centered at about 0.5 mb (approximately 54 km). Figure 6.2b gives the weighting functions for these synthesized channels.

The consistency between the TOVS channels has been examined by computing the difference between the zonally averaged radiances obtained for the north- and southbound portions of the orbit at each latitude. Because the NOAA spacecraft are in Sun-synchronous orbits, the nadir-view observations at a given latitude are always for fixed local times, which are about 12 hours apart at most latitudes for a given spacecraft. Observation local times were about 0300 and 1500 hours for TIROS–N, NOAA–7, and NOAA–9, and about 0700 and 1900 hours for NOAA–6 and NOAA–8. The existence of diurnal and semidiurnal solar tides is a major complication because they lead to consistent biases between the measurements at these various local times. A solar diurnal tide will cause a difference between the north- and southbound zonal means, but will not affect their average except when their local times differ substantially from 12 hours. However, a solar semidiurnal tide has the reverse effect of causing a bias in the north/southbound average, but producing zero difference in the zonal means. The lunar semidiurnal tide has an effect similar to that of the solar semidiurnal tide, except that it has a 4-week periodicity; its effect was eliminated here by averaging over monthly periods. For the diurnal cycle, which has the largest

amplitude at extratropical latitudes, solar tidal theory predicts maximum 12-hour differences of less than 0.3K at 100 mb, less than 0.5K at 20 mb, and rising to a peak of about 6K at 2 mb. The temperature is predicted to peak at about 1800 hours. The TOVS observations are compatible with this theory. Not only are the 12-hour differences as expected (larger for the 0700–1900 hour spacecraft), but so are the absolute differences between spacecraft.

For trend determination, it is important to distinguish between radiometric calibration and spectroscopic errors, which are largely independent. A single channel will measure radiance (or brightness temperature) corresponding to a weighting function. Radiometric calibration errors cause the measured radiance to be incorrect, directly causing a temperature error. Spectroscopic errors (such as errors in the filter wavelength or in the basic spectroscopic line data) will cause errors, such as a vertical shift, in the weighting function; this leads indirectly to temperature errors that will depend upon the lapse rate and, hence, upon the latitude and season. Both types of error have various components of systematic bias, but some of these will be common to all instruments of a given type or design. Thus, errors in spectral line data would be unimportant when intercomparing SSU's, but would matter when comparing an SSU with an MSU, since the two instruments view at quite different wavelengths. Nash and Forrester (1986) used measurements of natural atmospheric variations that are height dependent (e.g., the tidal 12-hour difference, seasonal variations) to intercompare the pressure levels viewed by different radiometers and by radiosondes, and so establish which channels were observing at the correct level. Residual differences were then described as biases. The latitudinal variation of bias between the different measurements for the same pressure level was also used as an indication of data quality and of the types of instrument problems that could be occurring. Of crucial importance was the apparent long-term stability of the NOAA–6 SSU and MSU. Although there were periods when this satellite was not operated (because of the failure of the HIRS–2), there was enough overlap of operation with other NOAA satellites to be confident of the long-term trends shown. Temperature values within these gaps were obtained from TOVS instruments on the other satellites, after adjustments were made for identifiable radiometric and spectroscopic differences.

The overall conclusions regarding the accuracy of TOVS data for long-term trend studies are:

- Single TOVS channels can, in some cases, measure monthly zonal mean brightness temperature to an accuracy of about 0.2K root mean square (rms) (1K for synthesized channels).

- The data sets obtained from several satellites indicate that the NOAA–6 SSU and MSU were stable over the period 1980–1986 to the same order of accuracy.

Because the atmospheric mixing ratio of carbon dioxide is increasing at a rate of about 0.4 percent per year, the weighting function for a spectroscopically stable SSU channel moves upwards, causing a change in the measured brightness temperature that depends on the lapse rate. Line-by-line calculations have been made of the effects of an 8 ppmv increase in the carbon dioxide mixing ratio, corresponding to the change from 1979–1980 to 1985–1986, for an annual mean 30°N temperature profiles. These changes (listed in Table 6.1) are substantially smaller than the trends observed, so it is concluded that these effects play only a minor role. Oxygen mixing ratios are proportionally much more stable than those of carbon dioxide, and any trend for the MSU weighting functions should be negligible. Another potential source of error is the effect of ozone upon absorption in the 15-micron carbon dioxide band used by the SSU and HIRS for temperature sounding. The use of gas correlation minimizes the effect of ozone on the SSU measurements to the extent that it is not considered necessary to make any correction. However,

Table 6.1   Sensitivity of Measured SSU Brightness Temperatures to 8 ppmv CO_2 Increase and 10 Percent Ozone Decrease at all Levels

Channel	Apparent Temperature Increase Due to 8 ppmv CO_2 Increase (K)	Apparent Temperature Increase Due to 10% Ozone Decrease (K)
47X	−0.289	−0.01
36X	−0.072	−0.04
27	0.00	0.00
26	0.12	−0.01
25	0.14	−0.02
26X	0.182	0.02
15X	0.085	0.05

Table 6.1 gives the calculated apparent temperature changes caused by a 10 percent decrease of ozone concentration. Any small ozone trend that might have occurred should have negligible effect on the temperature trend measurements over this period. The corrections indicated in Table 6.1 have not been incorporated into the data set's satellite.

6.2.2.3 NMC Analyses

The NOAA series of polar-orbiting satellites has provided temperature soundings in support of operational meteorological analyses for weather forecasting. As part of the regular operations of the NMC, global fields have been produced of geopotential height and temperature at stratospheric constant pressure levels 70, 50, 30, 10, 5, 2, 1, and 0.4 mb (corresponding to altitudes from 18 to 55 km). The analysis system for the fields is a modified Cressman for both 70 to 10 mb levels (Finger et al., 1985) and 5 to 0.4 mb levels (Gelman and Nagatani, 1977). The source of satellite data for the analysis, as well as the methodology for using these data in the analysis system, have changed as improvements have been developed (Gelman et al., 1983). Some changes were necessary because of instrumental failure or failure of specific instrument channels. Table 6.2 summarizes the principal changes that are relevant to a study of the stratospheric fields (70 to 0.4 mb) for the Northern and Southern Hemisphere analyses. The changes to the 70 to 10 mb system primarily have involved changes in the use of radiosonde data for the Southern Hemisphere and in first-guess derivation. Changes for the upper stratosphere (5 to 0.4 mb) analyses relate to changes in satellites as well as in the use of TOVS data. Before October 17, 1980, simple regression relationships from two channels of the VTPR or the SCR were used. Temperature retrievals produced from TOVS provide layer mean temperature between the standard pressure levels. Temperatures at the NMC analysis levels are found by linear interpolation in log pressure of the layer mean temperatures.

As indicated in Table 6.1, there have been seven changes (eight periods) since the initiation of the NMC global stratospheric analyses. Some basis must be provided for assuring stability of the NMC analyses for determining interannual changes in stratospheric structure and long-term trends in temperature. Therefore, meteorological rocketsonde and radiosonde temperatures have been compared with temperatures interpolated to the locations of the rocket stations from the analyzed field closest in time.

The error estimates for rocketsonde temperature data are 1–3K over the altitudes 35 to 55 km (see Section 6.2.3). Since both rocketsonde hardware and data observation procedures have been standardized for the stations in the Cooperative Meteorological Rocketsonde Network (CMRN)

Table 6.2 Global Daily 1200 GMT Temperature and Height Fields History of Changes

Period	Dates	Levels (mb)	Hem.	Data and Analysis Procedures
1	Sept. 24, 1978–Feb. 23, 1979	70–10	N	Rawinsonde data First guess 50% persistence, 50% regression upward
		70–10	S	Radiosonde and VTPR temperatures
		5–0.4	N,S	Regression from VTPR channels 1,2
2	Feb. 25, 1979–Oct. 16, 1980	70–10	N	Rawinsonde data
3	(2/25/79–1/20/80; TIROS–N) (1/21/80–10/16/80; NOAA–6)			First guess 50% persistence, 50% TOVS beginning Oct. 3, 1979
		70–10	S	Radiosonde and TOVS temperatures
		5–0.4	N,S	Regression from SSU channels 25,26
	Oct. 17, 1980–Present	70–10	N	Rawinsonde data
4	(10/17/80–9/1/81; NOAA–6)			First guess 100% TOVS beginning 17 June 1981
5	(9/2/81–9/1/83; NOAA–7)			TOVS first guess saved outside
6	(9/2/83–6/18/84; NOAA–8)			NMC octagon grid
7	(6/19/84–2/26/85; NOAA–7)			points beginning 29 Feb., 1984
8	(3/27/85; NOAA–9)			
		70–10	S	TOVS (no radiosonde)
		5–0.4	N,S	TOVS

since at least 1978, an inherent assumption is made that these rocketsonde data may be used as a reasonable and consistent standard against which to gauge the long-term stability of the NMC stratospheric temperature analyses.

Adjustments have been derived and applied to the archived NMC stratospheric analyses for 5 mb and above. The temperature adjustments are, at most, 9K; the largest adjustments occur nearest the Equator or the North and South Poles. The adjustments are recommended for application in the Southern as well as in the Northern Hemisphere, even though the rocketsonde stations used to derive the adjustments are almost exclusively in the Northern Hemisphere. This puts significant limitations on Southern Hemisphere trend estimates.

Another approach to deriving adjustments is to determine directly the difference between analyses obtained from the two data sources. It is best if an overlap period, during which comparisons can be made of the two analysis products, is available. This has not been possible in the past because of operational considerations at NMC. Furthermore, some changes needed as a

result of the failure of an instrument or specific channels precluded such an overlap period. Therefore, Gelman et al. (1983) compared zonal average temperatures derived from the analyses immediately before and after each change and tried to determine the nonmeteorological change at each change date. This determination is most difficult at polar latitudes in winter and may not be possible when there is a lapse in analyses of more than a few days, as was the case at the beginning of period 8. Figure 6.3 shows these determinations (denoted by joint) for the Equator, 30°N, 30°S, 60°S, and 60°N for the 2-mb level over the eight adjustment periods (see Table 6.2). Figure 6.3 (denoted by Rocket) also shows the changes implied by the rocket comparisons.

Another method of estimating these changes is by statistical evaluation. Estimates based on this approach for 2 mb are also shown in Figure 6.3 (denoted by Step Regression) and are discussed in detail by Gelman et al. (1983). The pattern of relative agreement among the different methods depicted in Figure 6.3 is reasonably good. However, differences of 2–4K are common, and uncertainty in adjustments of this magnitude should be expected.
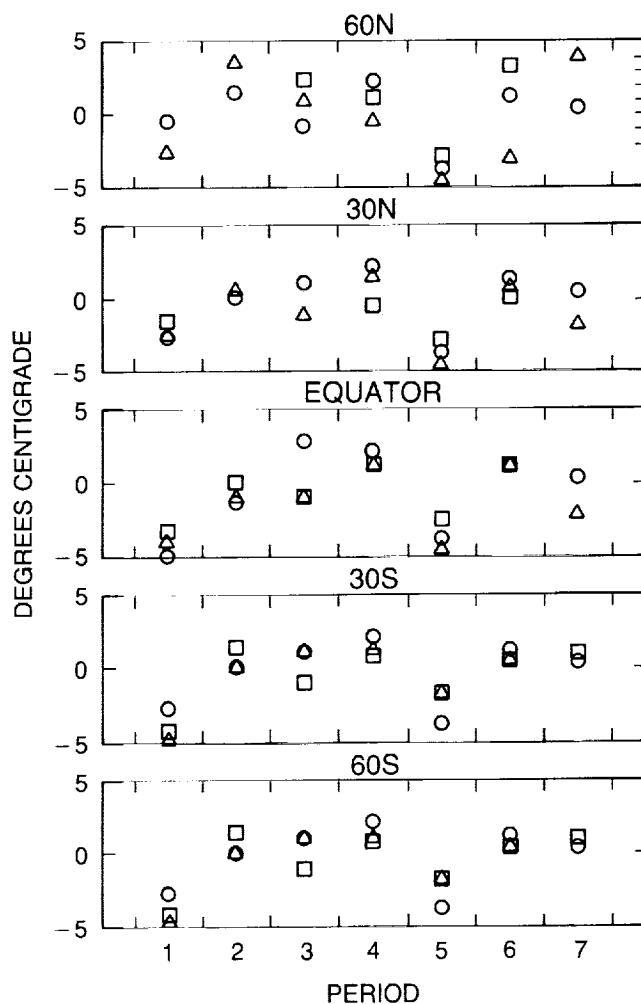

Figure 6.3 Temperature changes in the 2 mb NMC analyses, as inferred from rocket comparisons (○, Rocket), comparison of analyses around change dates (□, Joint), and regression (△, Step Regression), as explained in text.
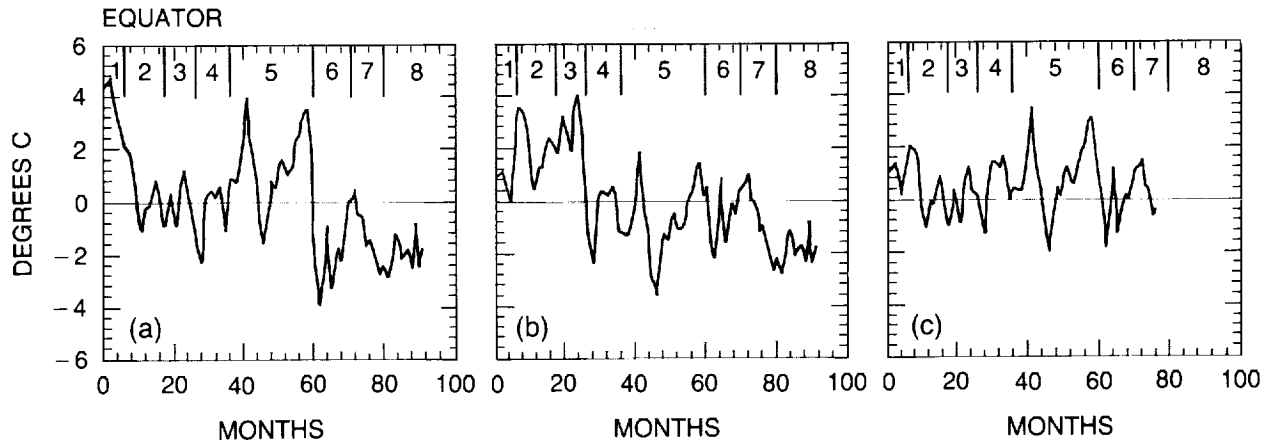
EQUATOR

Figure 6.4 Monthly 2 mb average temperature (a, unadjusted; b, adjusted to rocket; c, adjusted to joints) deviations from the long-term monthly averages for the Equator. Time runs from October 1978 (month 1) to April 1986 (month 91).

Figure 6.4a shows the unadjusted 2-mb equatorial deviations for the 91-month period of record. Large changes in the level of deviations may be noted between several of the periods. In Figure 6.4b, the 2-mb equatorial deviations are shown after adjustments for rocket data comparisons have been applied. A jump of about 2K may be noted between periods 3 and 4; the reason is not yet known. Figure 6.4c shows the 2-mb equatorial deviations after the adjustments, using the method of joints (Gelman et al., 1983), have been applied. The jumps between periods have been largely eliminated by this method. However, no joint adjustment was derived between periods 7 and 8 because good analyses are lacking as a result of noisy SSU data on NOAA-9. It is also noted that this result is consistent with Figure 6.3, in which the changes from periods 3 to 4 are consistent between the joint and statistical methodologies, but differ from the rocketsondes. The cause of this discrepancy is under study, but it points out the need for consistent ground truth and the efficacy of a system of checks and balances. Figure 6.5 shows comparable information for 30°N. For this and other latitudes, after rocket adjustments have been applied, unexplained jumps are less apparent than for the Equator.
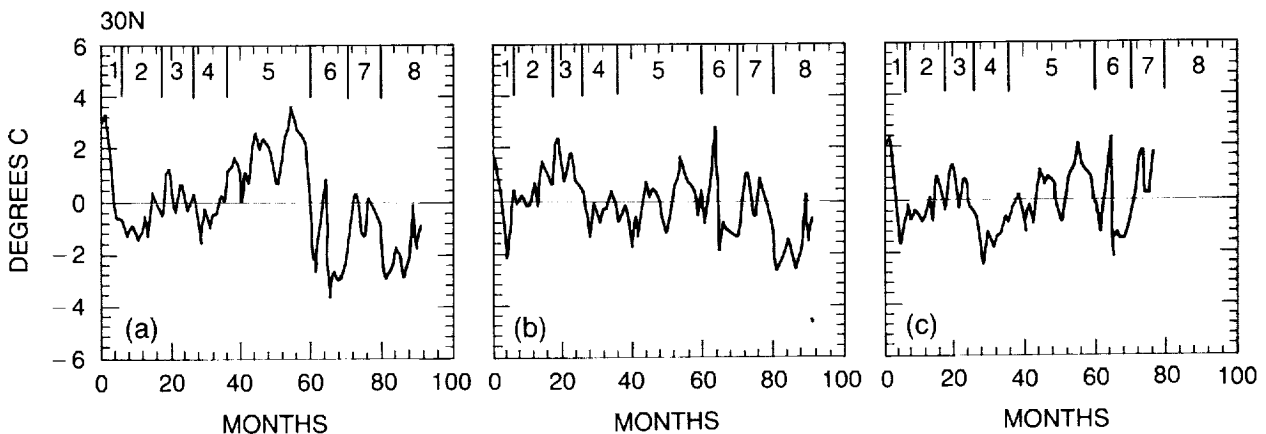
30N

Figure 6.5 As in Figure 6.4, but for 30°N.

457

The underlying theme of this discussion has been to determine to what degree a trend in stratospheric temperature can be detected. On average, NMC analyses have had one major change a year with a confidence factor of 2–3K. Thus, if NMC stratospheric analyses with current adjustment techniques are used, a trend of less than 1.5K per decade over a decade would not be detected; however, a decadal change of 4–5K would be detectable.

6.2.3 Rocketsonde

6.2.3.1 Introduction

The number of rocketsonde launch sites operated by the United States increased from an initial 3 or 4 sites in 1958 to about 30 in 1965, and has since decreased to the present 9 sites. The number of rocketsondes launched in the U.S. has also decreased, from 3 to 5 per week to about 3 to 5 per month—a serious limitation for detecting long-term trends.

Despite the long period of rocketsonde measurements that exists for the U.S., many of the launch sites are unsuitable for trend analysis because of short, and often incomplete, data records. Nonetheless, the U.S. rocketsonde program has provided sufficient information from 14 launch sites (Table 6.3) to attempt an analysis of temperature trends. For this report, six sites with the most complete long-term records will be discussed.

6.2.3.2 Corrections

When properly applied, rocketsonde temperature corrections should improve the estimate of ambient temperature. Examples of optimal corrections applied to the Arcasonde and Datasonde instruments are presented in Table 6.4 and applied to the same temperature profile, independent of the instrument. The aerodynamic and radiation corrections are the dominant contribution to the total correction.

Table 6.3 Rocketsonde Launch Sites Having Data Available for Trend Analysis

Rocketsonde Site	Latitude	Longitude	Observational Period
Ascension Island	9°S	14°W	1969–1985
Kwajalein, MI	9°N	168°E	1979–1985
Ft. Sherman, CZ	9°N	80°W	1969–1979
Antigua, BWI	17°N	62°W	1969–1977
Barking Sands, HI	22°N	160°W	1969–1982
Cape Canaveral, FL	28°N	81°W	1969–1986
White Sands Missile Range, NM	32°N	106°W	1969–1982
Pt. Mugu, CA	34°N	119°W	1969–1982
Wallops Island, VA	38°N	75°W	1969–1980
Shemya, AK	53°N	174°E	1975–1985
Primrose Lake, Canada	55°N	110°W	1969–1982
Ft. Churchill, Canada	59°N	94°W	1971–1979
Poker Flat, AK	65°N	148°W	1969–1978
Thule, Greenland	77°N	69°W	1976–1981

NOTE: Data exist into 1986 for most of these sites. However, the reduction in the number of the U.S. rocketsonde launchings beginning in the late 1970's inhibits analysis outside of above dates.

Table 6.4 Example of Arcasonde and Datasonde Measurements of Same Temperature Profiles and Appropriate Corrections

	Temp. (K)	Aero. Heating	Lag.	Emissivity	Radiation	Correction	Ambient Temp.
Alt. = 40 km							
Arcasonde	250.0	−0.4	−1.0	0.4	−0.4	−1.4	248.6
Datasonde	250.3	−0.4	−0.5	0.3	−1.1	−1.7	248.6
Alt = 45 km							
Arcasonde	242.0	−0.9	−1.2	0.5	−0.4	−2.0	240.0
Datasonde	242.6	−0.9	−0.7	0.4	−1.4	−2.6	240.0
Alt = 50 km							
Arcasonde	261.0	−2.1	−1.7	0.9	−0.5	−3.4	257.6
Datasonde	261.9	−2.2	−0.9	0.7	−1.9	−4.3	257.6

NOTE: Corrections are from Krumins and Lyons (1972).

The interpretation of the temperature trend between 1971 and 1973 given by Johnson and Gelman (1985) proposes that part of the sudden decrease in the temperature observed (~3K) could be attributed to a changeover in instrument design (i.e., from Arcasonde to Datasonde); however, the decrease is still present when only Datasonde profiles are used (Schmidlin, private communication). The Datasonde gradually replaced the Arcasonde at all U.S. ranges—at many before 1971. Krumins and Lyons (1972) published Datasonde corrections in 1972 that generally came into use at launch ranges in 1973. The initiation of corrections in 1973 might explain part of the decrease reported by Johnson and Gelman. The magnitude of the correction, if applied, would be about −1.0K at 40 km and about −1.6K at 45 km—approximately the amount of the difference noted between 1971 and 1973.

6.2.3.3 Rocket Data Base

All of the U.S. rocketsonde data available in the archive from 1969–1986 were examined. Data obtained before 1969 were not used because of the different data format. In addition, diverse instrument designs were used at some ranges until about 1971 and, in a few cases, even as late as 1973. Because the measurement quality of these systems varied from one instrument design to the other, the data from these instruments were not used. The rocket data base includes only Arcasonde and Datasonde data.

To eliminate the possibility of any discontinuity in the use of the corrections of Krumins and Lyons (1972) at any of the sites listed in Table 6.3, the data were examined for 1972 through 1986 to determine whether the standard U.S. correction was applied. If corrections had not been applied, they were incorporated. Furthermore, the temperature data obtained between 1969 and 1972 were also corrected using the same procedure. Thus, the temperature trend analyses presented here are produced from a consistent and homogeneous group of corrected temperature measurements extending from 1969 to the present.

It should be noted that even though the data set may now be considered uniform throughout, bad measurements were found in the profiles (as a result of bad calibrations or depressed

sensors, for example) and had to be eliminated. The data from the 14 sites selected for analysis were plotted with the accompanying conjunctive rawinsonde. Profiles that showed differences of 3K or more throughout their overlapping altitudes were subsequently deleted. No attempt was made to determine whether the fault was in the radiosonde or the rocketsonde data. The consequence of this editing was a reduction in the number of observations available for analysis by about 35 percent. Despite the removal of a large number of observations, sufficient data were available with a reasonable temporal distribution to produce the monthly averages used in the trend analysis.

The steps followed to obtain a valid and consistent data set for trend analysis can be summarized as follows:

- Only Arcasonde and Datasonde profiles from 1969 through 1986 were selected for analysis.

- All rocketsonde profiles from 1969 to 1972 were edited and quality checked by comparing them with the supporting radiosonde; if temperature differences of 3K or more were present, the rocketsonde observation was deleted.

- All uncorrected profiles were corrected, using the standard method.

6.2.3.4 Accuracy and Precision

Direct analysis of accuracy is difficult for rocketsonde instruments because of the lack of a reference standard. Although occasional Datasonde instruments give data profiles that disagree with the conjunctive radiosonde profile, a number of instruments were recalibrated after 2 years and found unchanged (Schmidlin, 1981). Thus, any disagreement between the rocketsonde and radiosonde temperatures is usually the result of bad calibration, an improperly mounted thermistor, or a bad radiosonde measurement. Poor data from these sources were removed as far as possible. However, true inflight accuracy is difficult to specify; hence, the need for corrections. Corrections should be known well enough to enable ambient temperatures to be produced from the thermistor temperature.

The accuracy of the Datasonde temperature sensor has been estimated as 3–5K, based on comparisons between 1) various rocket techniques (Olsen et al., 1979; Schmidlin, 1984), 2) rocketsonde instrument designs (Finger et al., 1975; Olsen et al., 1979), and 3) satellite instruments (Barnett et al., 1974; Barnett and Corney, 1984; and Pick and Brownscombe, 1981). A recent comparison of overlapping Datasonde thermistor and falling sphere measurements between 30 and 60 km (Schmidlin, private communication) revealed excellent temperature agreement to within the limits of the variability in the measurements. The inflatable sphere's measurement is independent of the external influences that disturb thermistor measurements (e.g., aerodynamic heating and radiation errors), so that this agreement suggests that Datasonde accuracy is probably near 1K up to an altitude of 60 km.

An analysis of paired measurements (Schmidlin, 1981) using 21 pairs of Datasonde, with the instruments of each pair launched 5 minutes apart, gave an estimate of repeatability of 0.8K at 35 km and 1.3K at 50 km. Through the use of an indirect method for estimating errors found in Gandin (1963), the precision of the Datasonde was calculated to be 0.6K at 35 km and 0.9K at 50 km.

460

6.2.3.5 Trend Detection

Initial trend analysis carried out for the 40 and 45 km altitudes using unedited Wallops Island and Cape Canaveral observations, respectively, indicated a temperature decrease of approximately − 0.35K per year. This rather large downward trend was determined for 1969–1986 using all of the data existing in the archive (including the unqualified rocketsondes, uncorrected profiles, and corrected profiles). Regression of the edited Cape Canaveral and Wallops Island monthly averages for the same altitudes showed trends of approximately − 0.22° per year and − 0.18° per year, respectively. Thus, the difference between the edited data used here and the unedited data can be very large.

Because of the sudden temperature decrease (between 1971 and 1973) reported by Johnson and Gelman (1985), it was considered important to attempt to determine whether the temperature drop originated from the Arcasonde to Datasonde changeover. Schmidlin (private communication) has separated Datasonde observations from all others in the 1970–1973 timeframe. From these Datasonde observations it is clear that a 2K drop in temperature still exists at most rocket stations. At the time of writing, it is still not clear whether this drop in temperature is due to undetected instrumental problems or to a real atmospheric change. Further work on this point is clearly warranted. Trends should be calculated separately for 1969–1986 and 1973–1986.

Since the sample size was reduced by about 35 percent after eliminating all suspect observations, as described above, there is some concern that the gaps between monthly averages were more frequent than desired and might lead to erroneous results. Consideration was given to using the longest complete data periods to reduce the error caused by the smaller segments of data. Only a handful of the 14 stations had sufficiently long data records to permit trend analyses. Trends were calculated between 1973 and the latest date possible for 4 of the 14 sites. The averages calculated for each altitude (30, 35, . . ., 55 km) are actually derived from 5-km vertical intervals (i.e., 30 km is an average of the temperatures between 28 and 32 km). Monthly averages are composed of the observations within a given month, with a minimum of three observations. When multiple observations occurred within the same day, only one observation for that day was included. Furthermore, it was important to reduce the effect that tidal activity might have had on the trend calculations. Therefore, only observations made in daylight were used. An attempt to use a more restricted time period of 2 or 4 hours centered about midday failed because then the sample size became too small.

6.2.3.6 Summary

A careful examination of the rocketsonde data for the 1969–1986 period, and elimination of the profiles that disagreed with the supporting radiosondes, reduced the data set by about 35 percent. If the standard U.S. correction had not been applied, the rocketsonde data were corrected following Krumins and Lyons (1972).

Monthly averages over the period 1969 to the end of the data set were calculated using daylight observations only; nighttime observations were avoided to reduce any biasing effect that might be created from the diurnal tide. Monthly averages comprise at least three observations. Johnson and Gelman (1983), using the unedited rocketsonde data, showed an average temperature decrease of 3.4K in the 25 to 30 km, 25° to 55°N region between 1970 and 1972, while the support radiosondes showed only a 2K change. However, the edited rocketsonde data set used here shows temperature decreases of 3.3K, 2.2K, 1.6K, 1.2K, and 2.9K at Cape Canaveral,

White Sands, Pt. Mugu, Wallops Island, and Primrose Lake over a 28 to 32 km altitude range for the same period. The average of these stations is in better agreement with the support radiosonde change, suggesting that the editing of biased rocketsondes and the application of corrections to uncorrected data may have alleviated much of the difference.

6.3 DATA ANALYSIS

6.3.1 Intercomparisons

In previous studies of stratospheric temperature trends, little attempt was made to intercompare data sets. The object of this section is to make the comparisons among the various data sets available for trend assessments and to provide a data quality check for long-term trend computations.

In a previous intercomparison study, Labitzke et al. (1986b) compared the radiosonde-based data of Angell and Korshover (1983a) (hereafter referred to as AK) to the Berlin analyses used by Naujokat (1981) (hereafter referred to as N (see Section 6.2.1.3 for a description of both data sets). Labitzke et al. (1986b) showed that some of the large differences between AK and N resulted from the omission of Russian radiosondes (i.e., the stations Orenburg, 50°N, 50°E; Omsk, 60°N, 70°E; and Kirensk, 60°N, 110°E) from AK's data before 1970, and from a few short periods between 1970 and 1978. Figure 6.6 (from Labitzke et al., 1986b) displays AK's data in the north temperate zone (solid line), the average of the 50°N and 60°N zonal means from the Berlin data (dotted line), and the average of points from the Berlin data collocated to the AK selected radiosonde sites (dashed line). The Berlin collocated data correspond well to the Berlin zonal means. The AK data do not correspond well to the Berlin data before 1970 and during the summer 1973 to summer 1974 period because of the absence of the Russian stations. During the 1978 through 1982 period, serious deviations between AK and the Berlin data occur that are ascribed by Labitzke et al. to missing or bad data.

The data sets used herein to make detailed comparisons are described in Section 6.2.2. Two of the data sets (satellite and NMC data) start in 1979; hence, the data sets for six levels in the
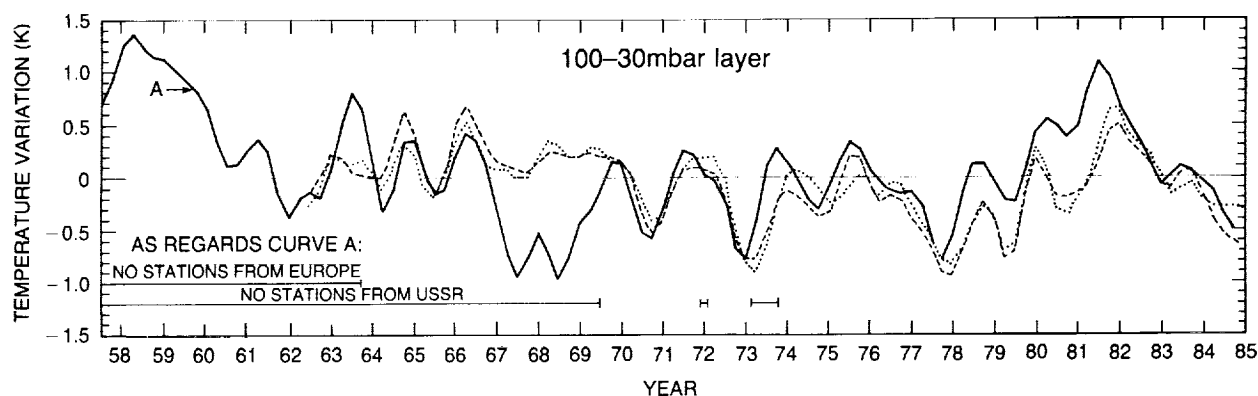

Figure 6.6   Temperature variation (K) in the 30–100 mb layer of "north temperate" latitudes, where a 1–2–1 weighting (1–1 at beginning and end of record) has been applied twice to successive seasonal deviations from the mean: ___ all stations from Angell and Korshover /7/ (mean 1958–1977); ---- all nearby grid points from Berlin analyses; . . . . average of the zonal mean of 50°N and 60°N from Berlin grid point data (mean 1963–1977); (tick marks are for summer = J–J–A).

stratosphere are compared, beginning from 1979 through 1986. Each data set has had the long-term seasonal average removed; these deseasonalized data have been smoothed with a 1-2-1 filter. The stratosphere has been divided into six levels (100 to 50 mb, 100 to 30 mb, 30 to 10 mb, 10 to 5 mb, 5 to 1 mb, and 0.5 mb) for the comparisons. The data are compared globally, in the Northern Hemisphere, in the Southern Hemisphere, and in the Tropics (30°S to 30°N).

Level Comparisons

100 to 150 mb

Figures 6.7a–d display the 100 to 50 mb layer mean temperature anomalies of the 1979 through 1986 period; the brightness temperature anomalies from MSU channel 24 centered at 90 mb (200 to 50 mb layer) (see Nash and Forrester, 1986), are also plotted. A visual comparison of the data set differences indicates a general consistency within 0.5K, that gives confidence in their reliability. The largest deviations within the data occur in AK's radiosonde data during 1985 in the Southern Hemisphere (Figure 6.7b). This data set is colder than those of the NMC and MSU by at least 1K. All of the data sets display the strong positive anomaly in late 1982 that has been associated with the eruption of El Chichón.
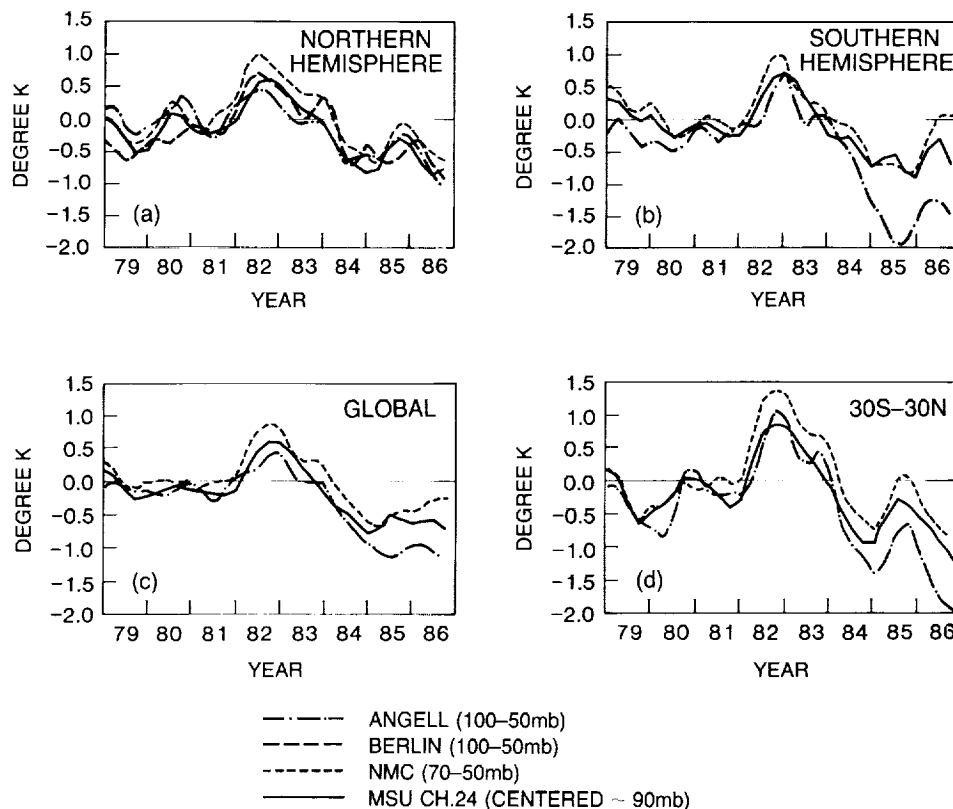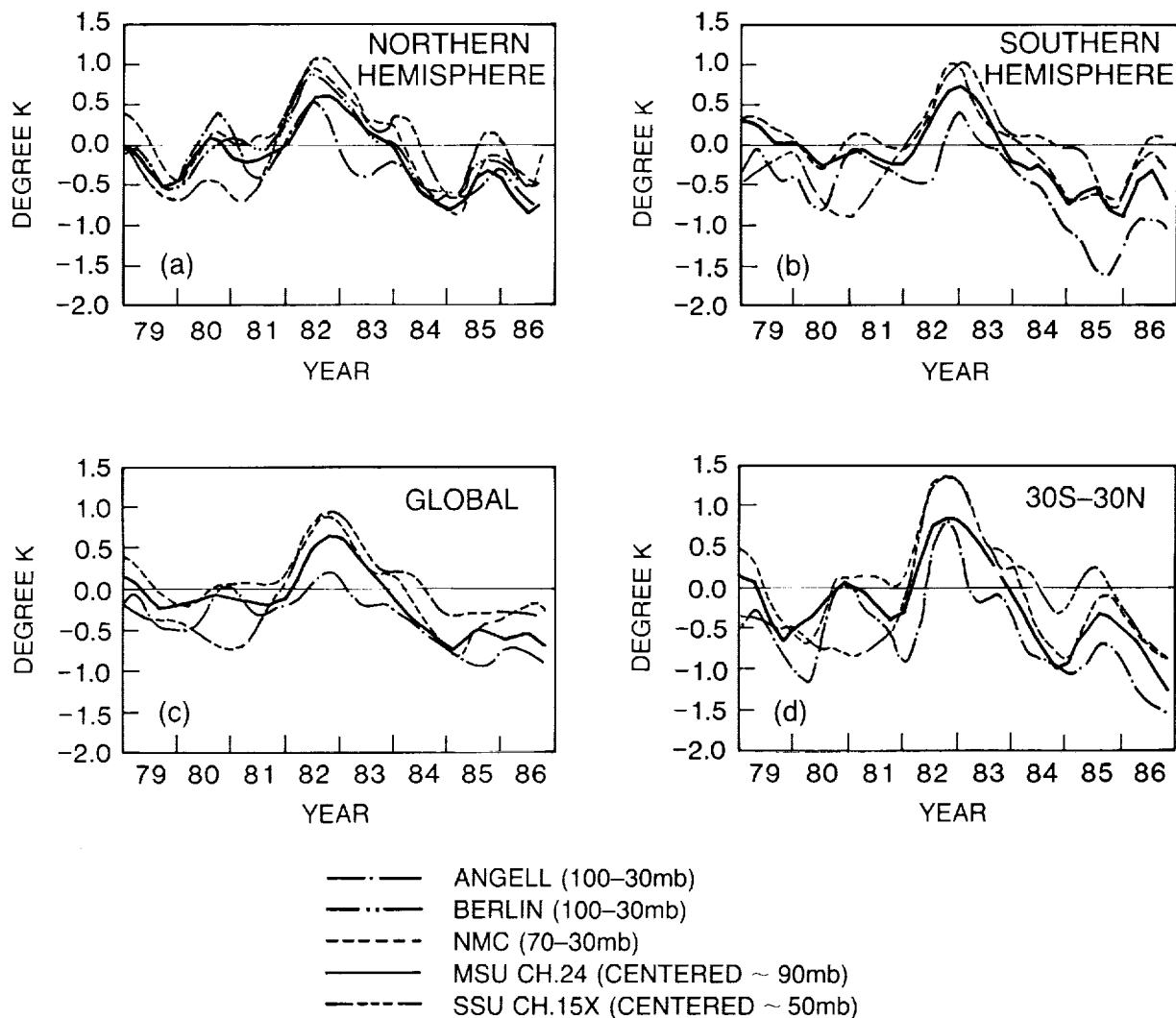

Figure 6.7   Seasonal temperatures with the long-term seasonal averages removed and smoothed 1–2–1 in time: Angell 100–50 mb radiosonde thickness (solid–dot); Berlin 100–50 mb thickness (long dash); NMC 70–50 mb thickness (short dash); and MSU channel 24 centered at approximately 90 mb (solid) for (a) Northern Hemisphere average, (b) Southern Hemisphere average, (c) global average, and (d) 30°S–30°N average. Berlin data were available only for the Northern Hemisphere. Tick marks on the abscissa correspond to the D–J–F seasons.

100 to 30 mb

Figures 6.8a–d display the 100 to 30 mb layer mean temperature anomalies for the 1979–1986 period. Two satellite channels are included here: MSU channel 24 (discussed previously), and SSU channel 15X centered at 50 mb (see Nash and Forrester, 1986). MSU–24 approximates the 200 to 50 mb layer mean temperature, while SSU–15X approximates the 150 to 20 mb layer mean temperature. These data are generally consistent to within 1K over the 8-year period. Comparisons between Figure 6.8 and Figure 6.7 show similar behavior. The most serious discrepancies between data sets occur with AK's data for 1985 (see Figure 6.7), and the SSU–15X data from 1980 and early 1981.


```
———·——   ANGELL (100–30mb)
———··——  BERLIN (100–30mb)
------   NMC (70–30mb)
———————  MSU CH.24 (CENTERED ~ 90mb)
-----    SSU CH.15X (CENTERED ~ 50mb)
```

Figure 6.8 Seasonal temperatures with the long-term seasonal averages removed and smoothed 1–2–1 in time: Angell 100–30 mb radiosonde thickness (solid–dot); Berlin 100–30 mb thickness (long dash); NMC 70–30 mb thickness (short dash); MSU channel 24 centered at approximately 90 mb (solid); and SSU channel 15X centered at approximately 50 mb (solid–dot) for (a) Northern Hemisphere average, (b) Southern Hemisphere average, (c) global average, and (d) 30°S–30°N average. Berlin data were available only for the Northern Hemisphere. Tick marks on the abscissa correspond to the D–J–F seasons.

30 to 10 mb

Figure 6.9 displays the NMC 30 to 10 mb layer temperature anomalies for 1979–1986 and SSU channels 26X (centered at 20 mb, solid line) and 25 (centered at 15 mb, solid-dot line). SSU channel 26X approximates the 55 to 7 mb layer, while channel 25 approximates the 50 to 5 mb layer. These data are generally consistent to within 1K. The NMC data are generally warmer than the satellite data from 1979 to 1983; they also show an extremely cold period during the Southern Hemisphere summer of 1985/1986, which is weakly apparent in the SSU channels.


```
------   NMC (30–10mb)
──────   SSU CH.26X (CENTERED ~ 20mb)
─ · ─ ·  SSU CH.25 (CENTERED ~ 15mb)
```
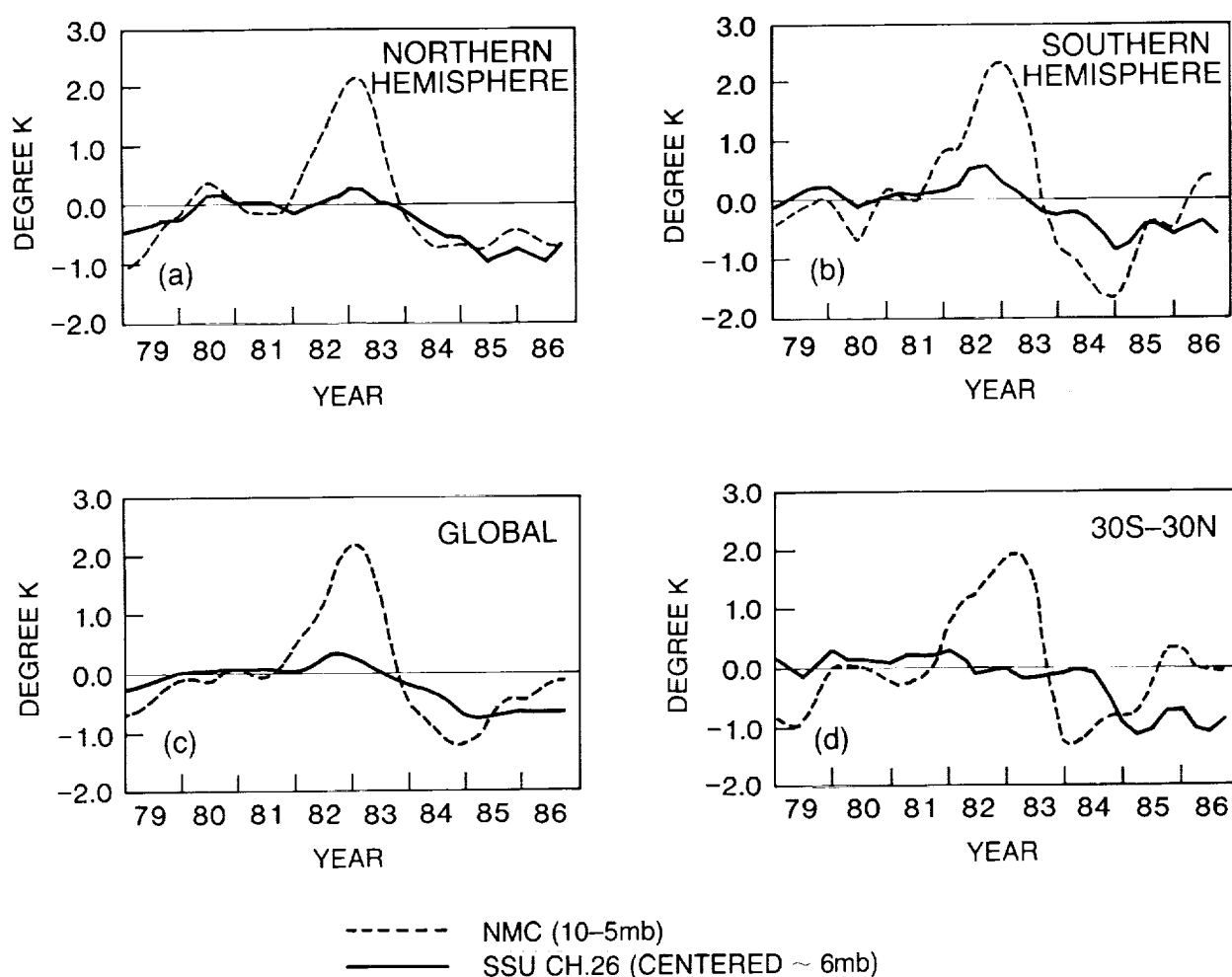
Figure 6.9 Seasonal temperatures with the long-term seasonal averages removed and smoothed 1–2–1 in time: NMC 30–10 mb thickness (dotted); SSU channel 26X centered at approximately 20 mb (solid); and SSU channel 25 centered at approximately 15 mb (three short dashes and a long dash) for (a) Northern Hemisphere average, (b) Southern Hemisphere average, (c) global average, and (d) 30°S–30°N average. Tick marks the abscissa correspond to the D–J–F seasons.

10 to 5 mb

Figure 6.10 displays the NMC 10 to 5 mb layer mean temperature anomalies and the SSU channel 26 data (centered at 6 mb and approximating the 20 to 2 mb layer). In general, the available data at this level are consistent only to 1–2K, and would produce radically different trends. For example, the NMC data show a 2K positive anomaly in both hemispheres during the 1982/1983 period, while the SSU data show weak positive anomalies on the order of 0.25–0.5K. Also note that a similar anomaly appears at lower levels in all of the data sets, but with a magnitude of only 1–1.5K.

Figure 6.10 Seasonal temperatures with the long-term seasonal averages removed and smoothed 1–2–1 in time: NMC 10–5 mb thickness (dotted); and SSU channel 26 centered at approximately 6 mb (solid) for (a) Northern Hemisphere average, (b) Southern Hemisphere average, (c) global average, and (d) 30°S–30°N average. Tick marks on the abscissa correspond to the D–J–F seasons.

5 to 1 mb

Figure 6.11 displays the NMC 5 to 1 mb layer mean temperature anomalies with SSU channel 27 (centered at 2 mb and approximating the 5.7 to 0.5 mb layer, solid line) and 36X (centered at 1.5 mb and approximating the 4 to 0.5 mb layer, solid-dot line) brightness temperature anomalies. Again, the NMC data show a strong positive anomaly between 1982 and 1983 that is not evident in the satellite data. The SSU data are very consistent with one another. Except for the 1982/1983 period, the data are generally consistent to within 1K of one another, and show a cooling of 1–2K between 1979 and 1986.
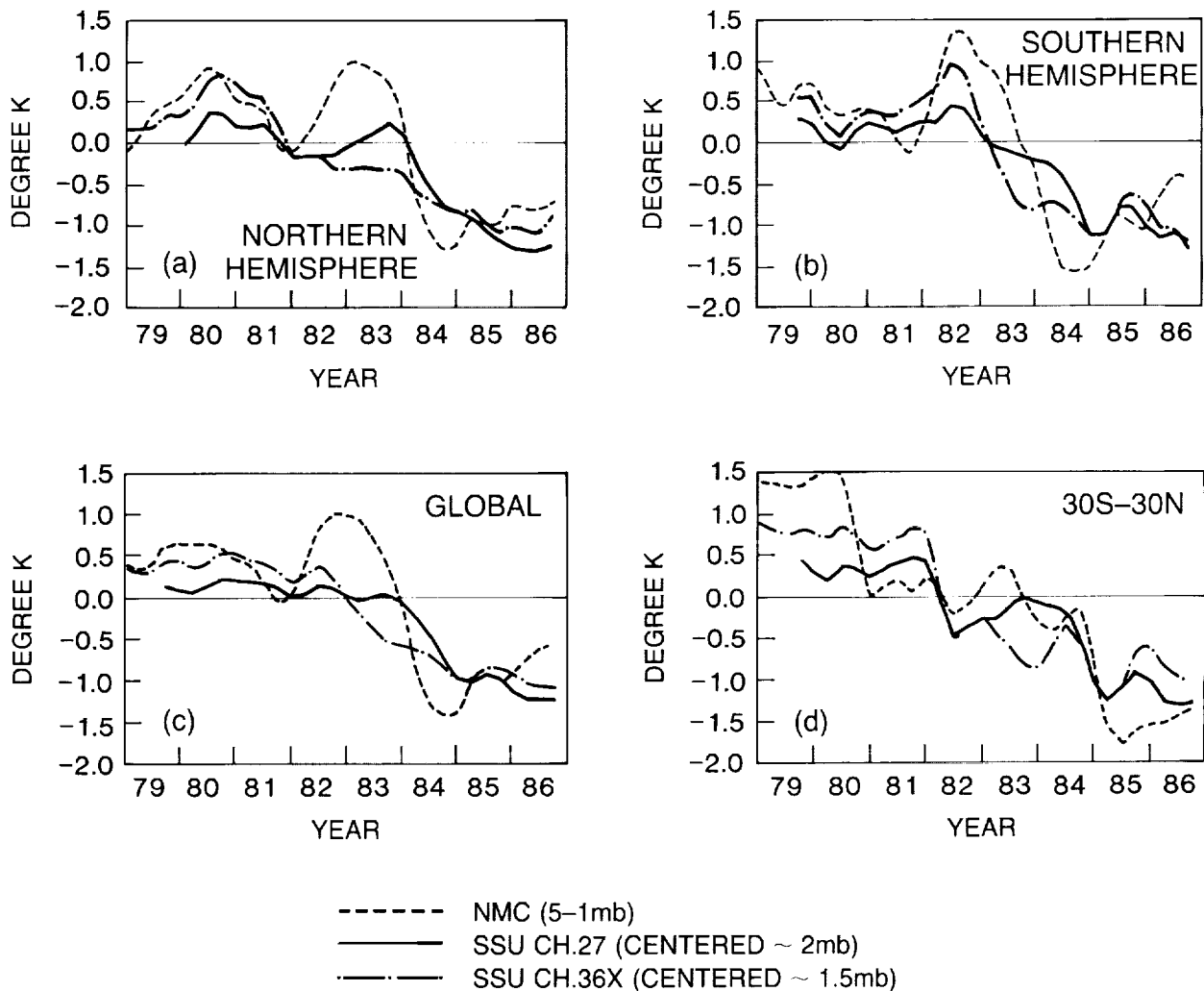


```
------ NMC (5–1mb)
——— SSU CH.27 (CENTERED ~ 2mb)
—·—· SSU CH.36X (CENTERED ~ 1.5mb)
```

Figure 6.11 Seasonal temperatures with the long-term seasonal averages removed and smoothed 1–2–1 in time: NMC 5–1 mb thickness (dotted); SSU channel 27 centered at approximately 2 mb (solid); and SSU channel 36X centered at approximately 1.5 mb (solid–dot) for (a) Northern Hemisphere average, (b) Southern Hemisphere average, (c) global average, and (d) 30°S–30°N average. Tick marks on the abscissa correspond to the D–J–F seasons.

467

0.5 mb

Figures 6.12a–d display the SSU channel 47X data centered at 0.5 mb and approximating the 1.2 to 0.2 mb layer. Few reliable data were available for comparison at this level, with the exception of the irregularly spaced rocketsonde data (see the following discussion). These data show an almost linear cooling of 2.5K from late 1979 to late 1986. Nash and Forrester (1986) estimate this channel to have a standard error of about 1K because of the sensitivity to changes in SSU channel 27's spectroscopic performance.

In addition to these conventional data sets, the data have also been compared to the rocketsondes (see Section 6.2.3). These rocketsonde data are irregularly spaced and are concentrated primarily in the Northern Hemisphere, with the exception of Ascension Island at 9°S, 14°W. Figures 6.13–16 display comparisons of rocketsonde and zonal mean satellite data from three stations at four different levels. These three stations (Ascension Island, 9°S to 14°W; Cape Canaveral, 28°N to 81°W; and Kwajalein Island, 9°N to 168°E) were chosen for the length and continuity of their data over 1979 to 1986.
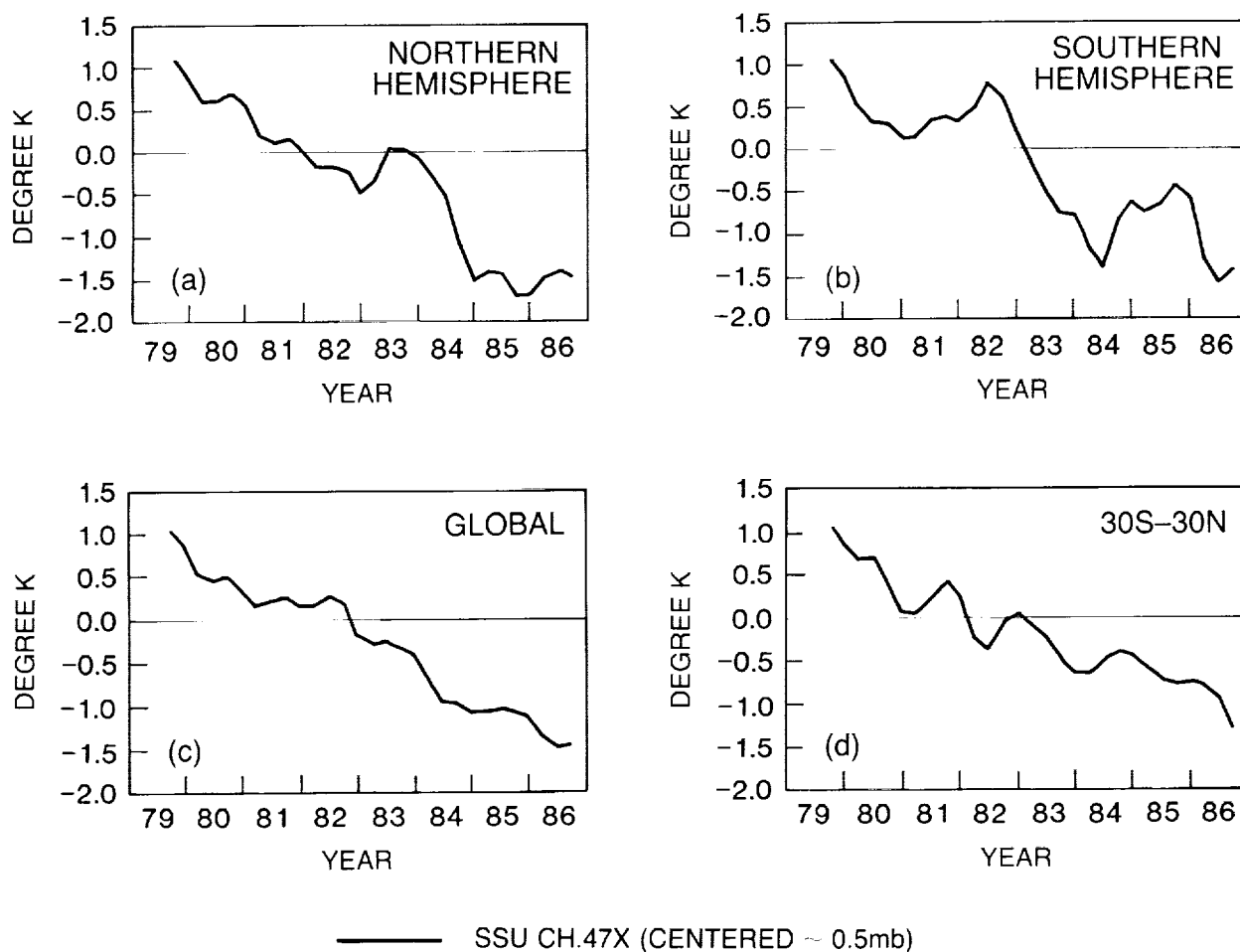

SSU CH.47X (CENTERED — 0.5mb)

Figure 6.12 Seasonal temperatures with the long-term seasonal averages removed and smoothed 1–2–1 in time for SSU channel 47X centered at approximately 0.5 mb for (a) Northern Hemisphere average, (b) Southern Hemisphere average, (c) global average, and (d) 30°S–30°N average. Tick marks on the abscissa correspond to the D–J–F seasons.

Figures 6.13a–c display rocket data averaged from 27.5 km to 37.5 km in comparison to the SSU channel 25 zonal mean data. SSU channel 25 is centered at 15 mb (~30 km), with a weighting function width of about 17 km. The Cape Canaveral data are compared to the 30°N SSU zonal mean; the Ascension data are compared to the 10°S SSU data; and the Kwajalein data are compared to the 10°N SSU data. The rocketsonde data are processed by finding the deviation from the long-term monthly mean, interpolating missing months, averaging the deviations into seasons, and, finally, smoothing the seasonal deviations with a 1–2–1 filter. In general, the data on these plots are consistent to only 1–2K. This poor consistency could result from the comparison of single station data to the satellite data zonal means. For example, all three rocket data sets show a strong quasi-biennial oscillation (QBO) signal that is largely absent from the SSU data at 10°S (Figure 6.13a) and 10°N (Figure 6.13c). A visual averaging of Kwajalein and Ascension shows that two large minima would still appear at the tick marks between 80/81 and 82/83—QBO minima at both stations. Nastrom and Belmont (1975) showed that the QBO has a 2K amplitude and is vertically deep (~20 km) in the region of SSU channel 25's weighting function; thus, this channel should have peak anomalies in excess of 1K. It is not clear why SSU channel 25 cannot resolve the QBO.
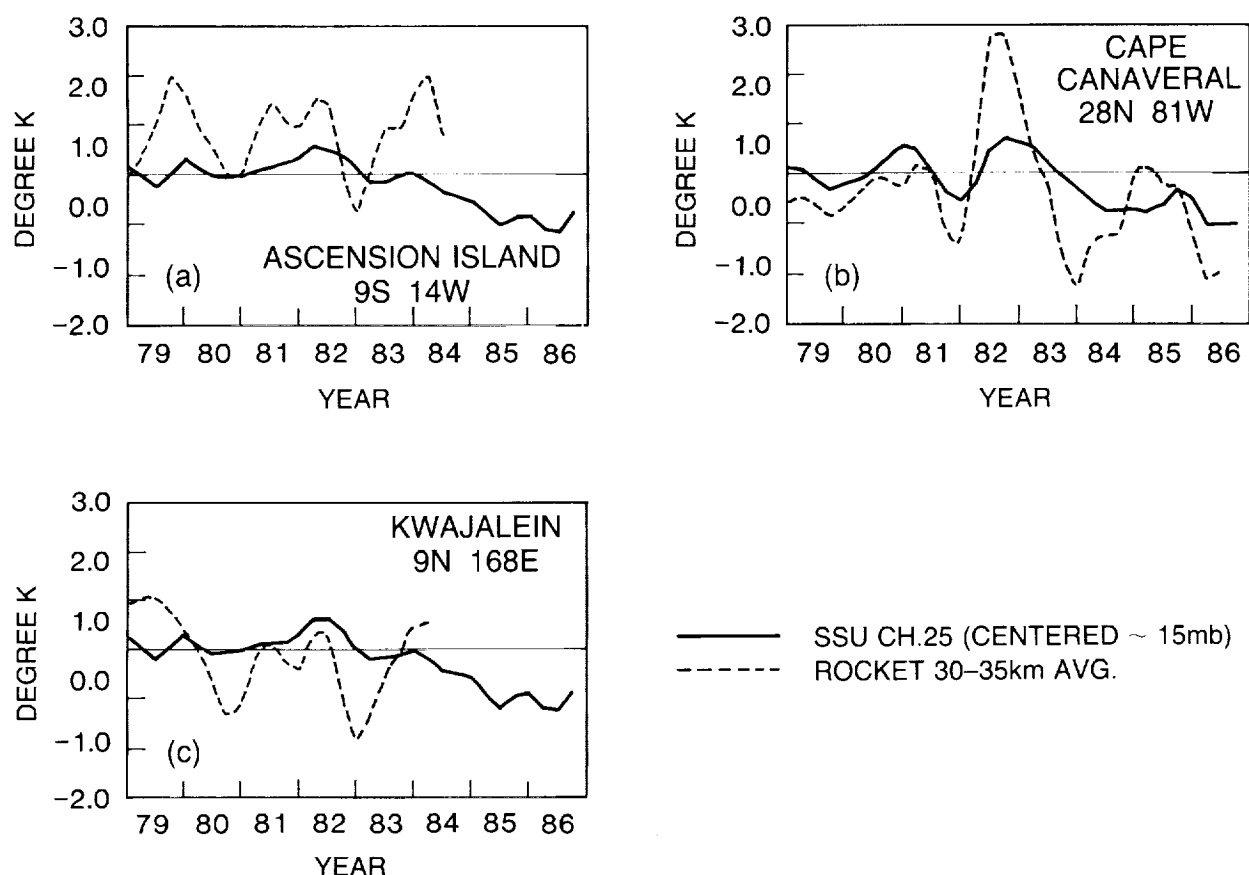

Figure 6.13 Seasonal temperatures with the long-term seasonal averages removed and smoothed 1–2–1 in time for the 30–35 km layer average of station rocket data (dotted) and the corresponding zonal average of SSU channel 25 centered at approximately 15 mb (solid) for (a) Ascension Island (9°S, 14°W), (b) Cape Canaveral (28°N, 81°W), and (c) Kwajalein (9°N, 168°E). Tick marks on the abscissa correspond to the D–J–F seasons.

Figure 6.14 displays the comparison of SSU channel 26 (centered at 6 mb or 35 km, with a weighting function width of 17 km) to the rocketsonde temperatures averaged from 27.5 km to 42.5 km. Again, the variations in this altitude range are greater in the rocketsonde data than in the satellite data, with a consistency of only 1-2K.

Figure 6.15 displays the SSU channel 27 (centered at 2 mb or 43 km, with a weighting function width of 17 km) layer temperature anomalies, SSU channel 36X (centered at 1.5 mb or 45 km, with a weighting function width of 12 km) layer temperature anomalies, and the 37.5 km to 52.5 km averaged rocketsonde temperature anomalies. These data sets are in very good agreement, with the exception of a strong positive anomaly at Cape Canaveral in mid-1982 that resulted from computer problems at Cape Canaveral in 1982 (K. Johnson, private communication). Coolings in all of the data sets from mid-1982 occur at both Ascension and Kwajalein in association with the El Chichón eruption. The data are consistent to 1K.

Figure 6.16 displays the SSU channel 47X (centered at 0.5 mb or 53 km, with a weighting function width of 17 km) layer mean temperature anomalies, and the 47.5 km to 57.5 km averaged rocketsonde temperature anomalies. The results of a comparison between these two data sets are not good; in general, they compare to within 1-2K.
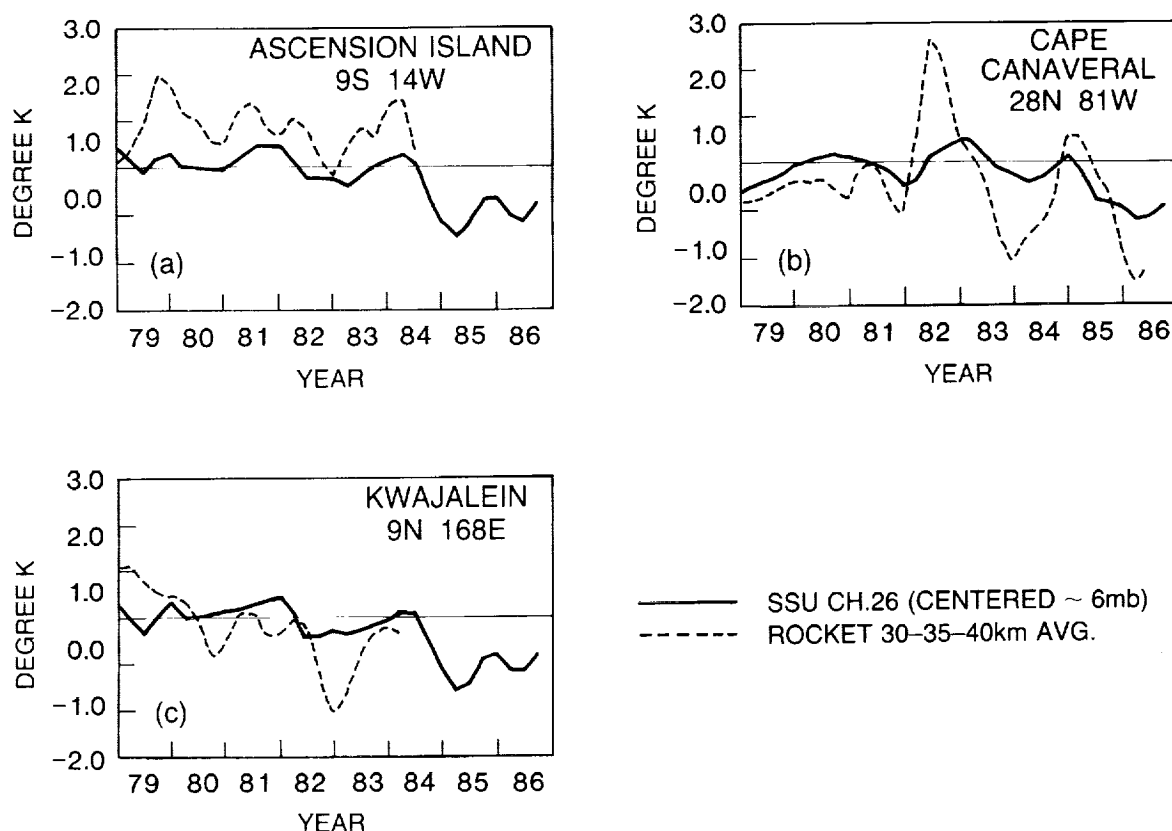

Figure 6.14   Seasonal temperatures with the long-term seasonal averages removed and smoothed 1–2–1 in time for the 30–35–40 km layer average of station rocket data (dotted) and the corresponding zonal average of SSU channel 26 centered at approximately 6 mb (solid) for (a) Ascension Island (9°S, 14°W), (b) Cape Canaveral (28°N, 81°W), and (c) Kwajalein (9°N, 168°E). Tick marks on the abscissa correspond to the D–J–F seasons.
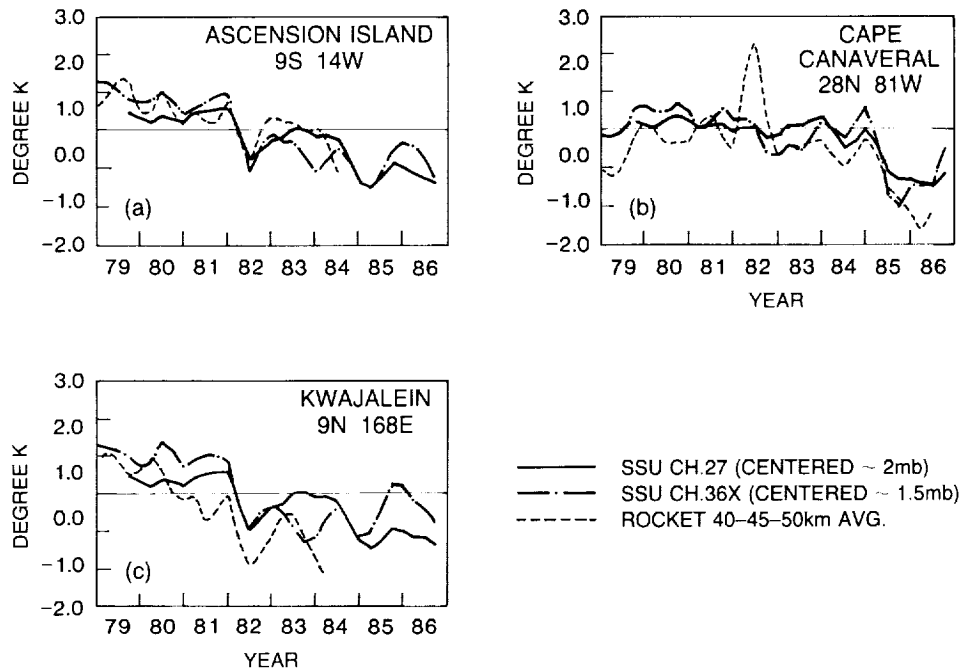
Figure 6.15 Seasonal temperatures with the long-term seasonal averages removed and smoothed 1–2–1 in time for the 40–45–50 km layer average of station rocket data (dotted) and the corresponding zonal average of SSU channel 27 centered at approximately 2 mb (solid) and SSU channel 36X centered at approximately 1.5 mb (solid–dot) for (a) Ascension Island (9°S, 14°W), (b) Cape Canaveral (28°N, 81°W), and (c) Kwajalein (9°N, 168°E). Tick marks on the abscissa correspond to the D–J–F seasons.
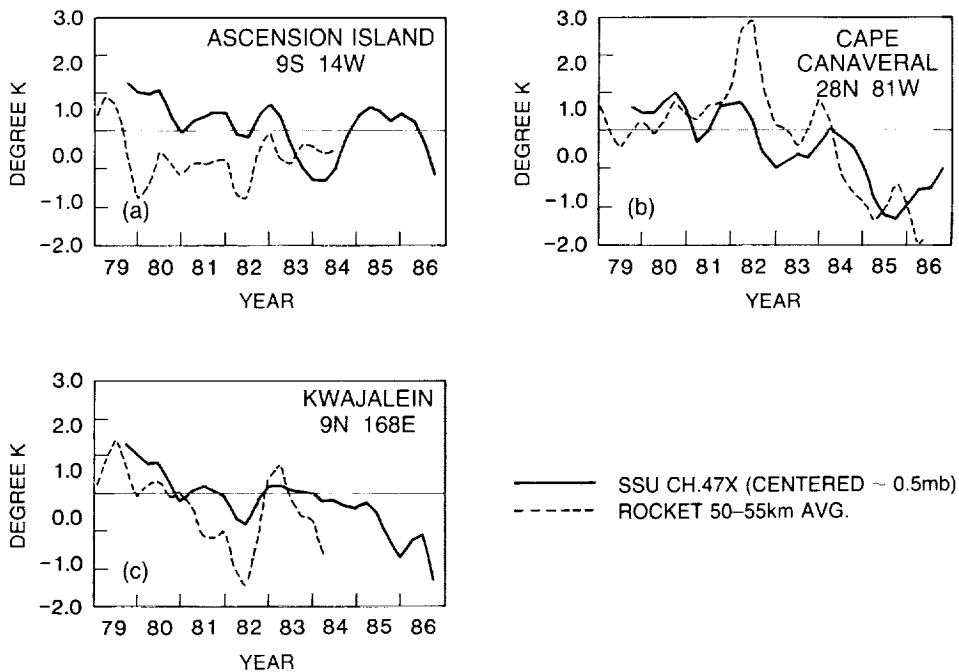

Figure 6.16 Seasonal temperatures with the long-term seasonal averages removed and smoothed 1–2–1 in time for the 50–55 km layer average of station rocket data (dotted) and the corresponding zonal average of SSU channel 47X centered at approximately 0.5 mb (solid) for (a) Ascension Island (9°S, 14°W), (b) Cape Canaveral (28°N, 81°W), and (c) Kwajalein (9°N, 168°E). Tick marks on the abscissa correspond to the D–J–F seasons.

6.3.2 Short-Term Change and Long-Term Trends

In the previous intercomparison section, effects on the data by the QBO and El Chichón are observed (e.g., see Figure 6.7d). These effects would tend to undermine trend computations. For example, the warming by El Chichón would tend to bias upward any trend computation that uses 1982 or 1983 data. Another technique for determining changes is to difference individual years; however, this technique would be biased by the respective phases of the QBO. To assess temperature changes that have occurred over the short period of 1979 to 1986, data from 1985 and 1986 have been averaged and differenced with the 1979 and 1980 average. This differencing avoids the 1982 and 1983 El Chichón event, while minimizing the QBO signal with the 2-year average.

The six levels used in the intercomparison section have been differenced; these differences are shown in Tables 6.5 to 6.10. The data sets used are the same as those shown in Section 6.3.1.

Figure 6.17 displays the global layer temperature changes over the 1979/1980 to 1985/1986 period as a function of altitude. The lower stratosphere shows a slight cooling of approximately 0.5K. The upper stratosphere (10 to 0.5 mb) shows coolings in excess of 1K. Recall that these changes are for layers that are on the order of 10 to 15 km deep. (See Figure 6.2 for the satellite weighting functions.)

Table 6.5 100–50 mb Layer Mean Temperature Changes 1986/1985–1980/1979

	N. Hem.	S. Hem.	Global	30°S–30°N
Angell Radiosonde	−0.6	−1.2	−1.0	−1.0
Berlin	−0.2			
NMC	−0.3	−0.6	−0.5	−0.2
MSU Channel 24 Centered at ~90 mb	−0.4	−0.6	−0.5	−0.5

Table 6.6 100–30 mb Layer Mean Temperature Changes 1986/1985–1980/1979

	N. Hem.	S. Hem.	Global	30°S–30°N
Angell Radiosonde	−0.3	−0.8	−0.6	−0.5
Berlin	−0.3			
NMC	−0.5	−0.5	−0.5	−0.4
MSU Channel 24 Centered at ~90 mb	−0.4	−0.6	−0.5	−0.5
SSU Channel 15X Centered at ~50 mb	0.2	0.1	0.1	0.2

Table 6.7 30–10 mb Layer Mean Temperature Changes 1986/1985–1980/1979

	N. Hem.	S. Hem.	Global	30°S–30°N
NMC	−0.6	−1.4	−1.0	−1.0
SSU Channel 26X Centered at ~20 mb[1]	−0.3	−0.6	−0.5	−0.8
SSU Channel 25 Centered at ~15 mb	−0.6	−0.6	−0.6	−0.9
Ascension Is.[2] (9°S, 14°W)	30 km			0.1
Cape Canaveral[3] (28°N, 81°W)	30 km			−0.7
Kwajalein[4] (9°N, 168°E)	30 km			−0.1

[1]The first period is the 2-year average September 1979–August 1981.
[2]The second period is the 2-year average August 1982–July 1984.
[3]The second period is the 2-year average September 1984–August 1986.
[4]The second period is the 2-year average July 1982–June 1984.

Table 6.8 10–5 mb Layer Mean Temperature Changes 1986/1985–1980/1979

	N. Hem.	S. Hem.	Global	30°S–30°N
NMC	−0.3	−0.2	−0.2	+0.3
SSU Channel 26 Centered at ~6 mb	−0.6	−0.6	−0.6	−1.0
Ascension Is.[1] (9°S, 14°W)	35 km			−0.1
Cape Canaveral[2] (28°N, 81°W)	35 km			−0.1
Kwajalein[3] (9°N, 168°E)	35 km			−1.3

[1]The second period is the 2-year average August 1982–July 1984.
[2]The second period is the 2-year average September 1984–August 1986.
[3]The second period is the 2-year average July 1982–June 1984.

Figure 6.18 displays the 30°S to 30°N layer temperature changes over the 1979/1980 average to 1985/1986 average period as a function of altitude. Three rocketsonde stations (Ascension Island, Cape Canaveral, and Kwajalein Island) are also included on this figure. Again, as in Figure 6.17, a small cooling is seen in the lower stratosphere, and a cooling of 1–2K in the upper stratosphere. The rocketsonde data tend to bracket the satellite data, thus illustrating the need for zonal averaging and showing that caution is needed when analyzing for trends at single stations.

The error bars used in Figures 6.17 and 6.18 are taken from the discussion in Section 6.2. The satellite data monthly zonal mean rms error is 0.2K (1K for synthesized channels), the daily

Table 6.9 5–1 mb Layer Mean Temperature Changes 1986/1985–1980/1979

	N. Hem.	S. Hem.	Global	30°S–30°N
NMC	−1.4	−1.5	−1.4	−2.8
SSU Channel 27 Centered at ∼2 mb[1]	−1.3	−1.2	−1.2	−1.5
SSU Channel 36X Centered at ∼1.5 mb	−1.4	−1.4	−1.4	−1.7
Ascension Is.[2]	40 km			−0.7
(9°S, 14°W)	45 km			−1.2
Cape Canaveral[3]	40 km			−0.3
(28°N, 81°W)	45 km			−0.5
Kwajalein[4]	40 km			−2.5
(9°N, 168°E)	45 km			−2.5

[1]The first period is the 2-year average September 1979–August 1981.
[2]The second period is the 2-year average August 1982–July 1984.
[3]The second period is the 2-year average September 1984–August 1986.
[4]The second period is the 2-year average July 1982–June 1984.

Table 6.10 0.5 mb Layer Mean Temperature Changes 1986/1985–1979/1980

	N. Hem.	S. Hem.	Global	30°S–30°N
SSU Channel 47X Centered at ∼0.5 mb[1]	−2.1	−1.4	−1.7	−1.3
Ascension Is.[2]	50 km			−0.6
(9°S, 14°W)	55 km			0.4
Cape Canaveral[3]	50 km			−2.0
(28°N, 81°W)	55 km			−2.3
Kwajalein[4]	50 km			−1.2
(9°N, 168°E)	55 km			−1.0

[1]The first period is the 2-year average September 1979–August 1981.
[2]The second period is the 2-year average August 1982–July 1984.
[3]The second period is the 2-year average September 1984–August 1986.
[4]The second period is the 2-year average July 1982–June 1984.

radiosonde based data should have errors on the order of 0.5K (based on the reproducibility of measurements; see Figure 6.1), the daily rocketsonde data have a repeatability of 0.8K (35 km) to 1.3K (50 km), and the NMC data errors are estimated from the daily radiosonde errors (0.5K in lower stratosphere) and daily rocketsonde errors (1.3K in the upper stratosphere). Monthly averaging should reduce the random errors in these data; hence, the error estimates for the rocket, radiosonde, and NMC data are very conservative. NMC errors are 1.5K at the upper levels.

The only data sets available for the longer term stratospheric trends are the Angell and Korshover (AK) radiosonde data, the Berlin data (B), and the rocketsonde data (R). The AK and B data (lower stratosphere) have been available only since 1970 and 1962, respectively. The R data (upper stratosphere and lower mesosphere) have limited spatial coverage.
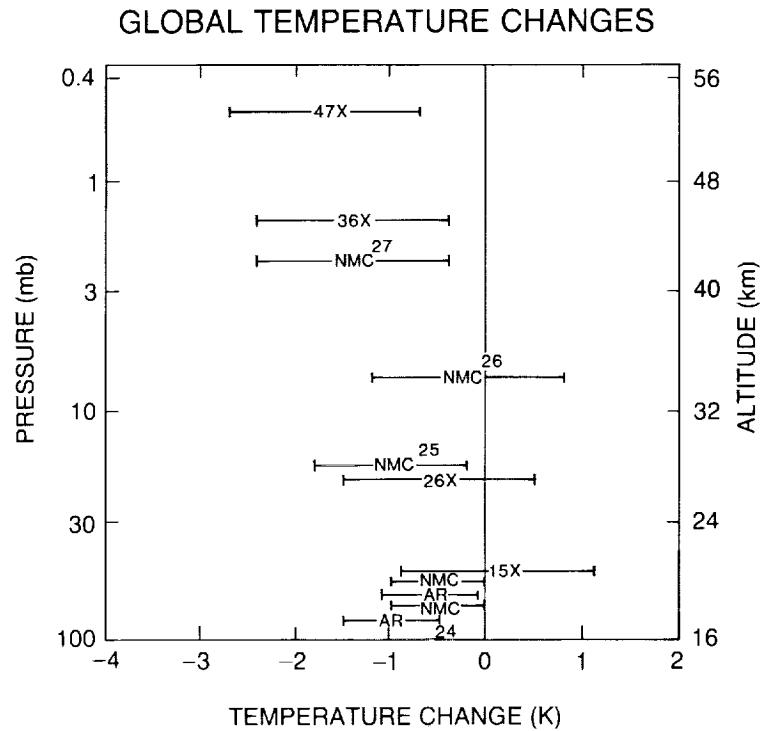
GLOBAL TEMPERATURE CHANGES

Figure 6.17 Summary of global stratospheric temperature differences (1985 and 1986 minus the average of 1979 and 1980). Symbols denote Angell's radiosonde data (AR), NMC data (NMC), and satellite data (channel numbers, see Figure 6.2). Error bars denote uncertainties (see text). Nash and Forrester (1986) estimate their satellite errors as 0.2 K rms (1 K rms for synthesized channels).
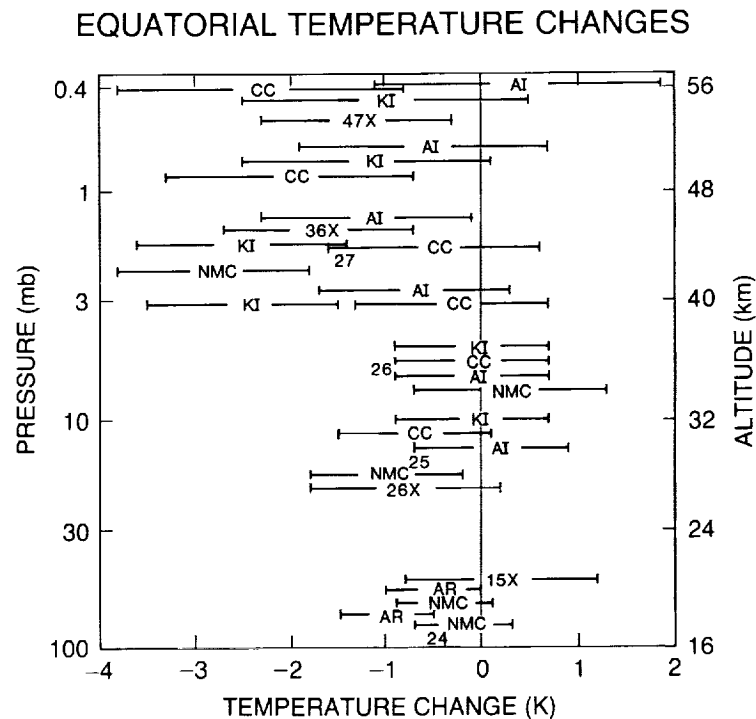
EQUATORIAL TEMPERATURE CHANGES

Figure 6.18 As in 6.17, except for Tropics and including rocket stations. Kwajalein Island (KI; 9°N, 168°E), Ascension Island (AI; 9°S, 14°W), and Cape Canaveral (CC; 28°N, 81°W).

475

Figure 6.19 displays the lower stratospheric trends of Angell and Korshover as well as the Berlin data. Both data sets are in good agreement within their error bounds. Figure 6.20 from Angell (1987) displays Northern Hemisphere combined radiosonde and rocketsonde trends from 1973 to 1985 for each season.

The trends above 25 km shown in Figure 6.20 are calculated from unedited rocketsonde data and are not in agreement with those computed from the edited data (see Section 6.2.3). In this report, trends computed from the edited rocket data are used. The monthly averaged edited data are processed by 1) computing the long-term monthly average, 2) removing those monthly averages, leaving the deviations from the monthly averages, 3) linearly interpolating missing data, 4) smoothing the data, and 5) using the smoothed data to compute two separate trends for the periods 1969 to data set end and 1973 to data set end. These monthly deviations (denoted by crosses), smoothed deviations (solid line), and least-square fits of the 1969–end smoothed deviations (straight line) are illustrated in Figures 6.21–26. The decadal trends for both 1969–end and 1973–end are shown in the lower right-hand corners of each graph.

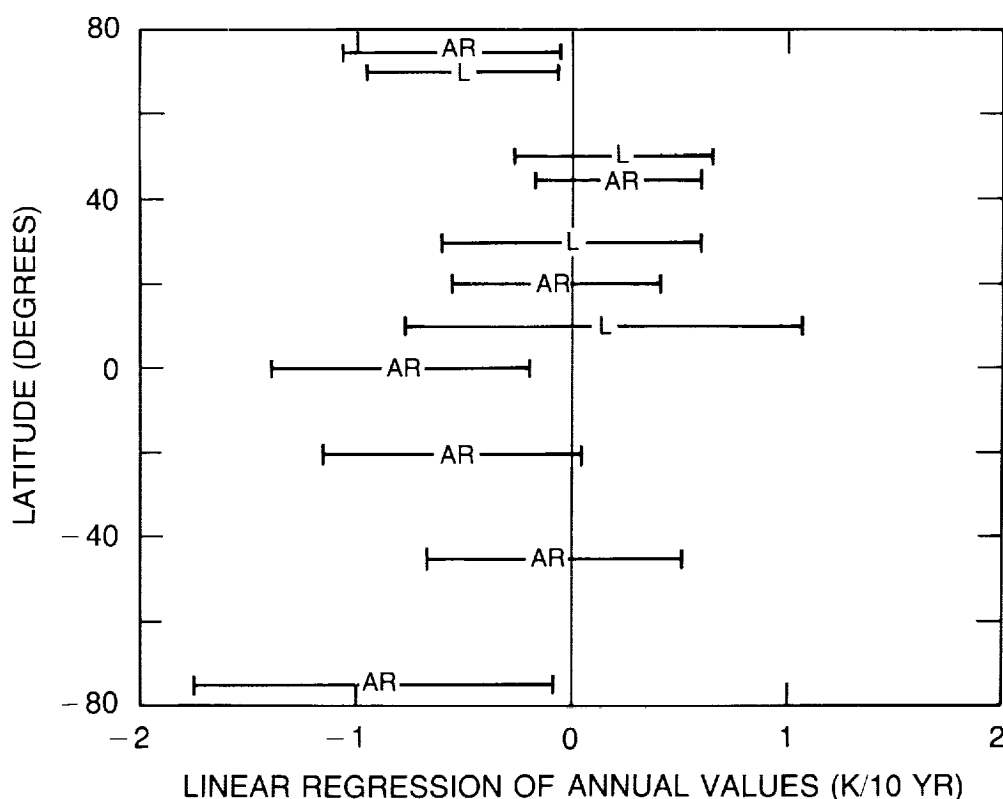## LOWER STRATOSPHERIC TEMPERATURE CHANGES

Figure 6.19   1970–1986 linear regressions from Free University of Berlin data at 30 mb (L), and Angell and Korshover (1983a) climate zones from the 100–30 mb thicknesses (AR). Error bars denote the 95 percent confidence limits of the regressions.

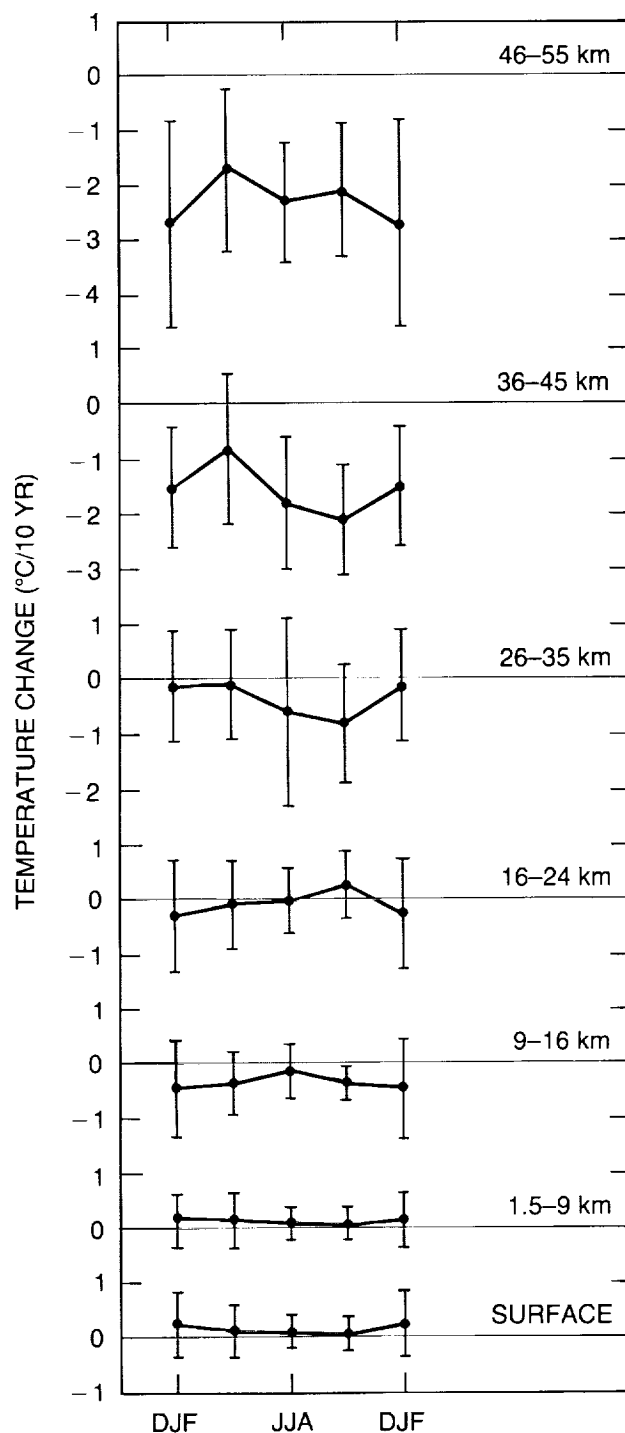SEASONAL CHANGES IN TEMPERATURE

Figure 6.20 Seasonal changes in tropospheric and stratospheric Northern Hemisphere temperature (degrees Celsius per 10 years) between 1973 and 1985 (DJF is December–January– February, etc.) based on linear regression applied to rocketsonde data primarily in the Western Hemisphere (values above 25 km) and radiosonde data around the entire hemisphere. The vertical bars are 95 percent confidence limits for the seasonal changes, as estimated from the standard deviation of seasonal temperatures about the line of regression.

Ascension Island (8°S)

Figure 6.21 depicts the monthly data and the trend for each of the six levels at Ascension Island. The trends observed at 30, 35, and 40 kilometers are large and positive. The trend is about −0.1K per decade at 50 km and −1.0K per decade at 55 km over 1973–1985. The QBO signal is seen in the data, with an amplitude of about 2K.

Kwajalein, Marshall Islands (9°N)

The Kwajalein data show evidence of the QBO signal at altitudes below 45 km with an amplitude of 1 to 2K. The 1973–1985 temperature trends for Kwajalein are small, as seen in Figure 6.22. At 30 km, the trend is only 0.7K per decade, while at 35 km to 55 km, the trends are even smaller.

Barking Sands, Hawaii (22°N)

The 1973–1982 trends calculated for Barking Sands also are small. Figure 6.23 shows that the rate of temperature decrease is, at 30 km, 0.8K per decade; at 35 km, −0.6K per decade; at 40 km, 0.3K per decade; and at 45 and 50 km, 0.3K and 1.9K per decade, respectively. At 55 km, the rate of increase is larger: 1.0K per decade. The temporal temperature structure at Barking Sands shows the QBO with a 1 to 2K amplitude.

Cape Canaveral, Florida (28°N)

Weak downward trends from 1973–1985 are noted at all altitudes, with the exception of 55 km. For example, Figure 6.24 shows downward temperature trends of −0.2K per decade at 30 km, −0.6K per decade at 35 km, −1.0K per decade at 40 km, −0.7K per decade at 45 km, and −0.6K per decade at 50 km. The QBO is again clearly seen, with an amplitude of 1–3K.

Pt. Mugu, California (34°N)

The Pt. Mugu 1973–1982 temperature trends (Figure 6.25) vary between no trend at 35 km to a 2.3K per decade trend at 55 km. A weaker (1K amplitude), chaotic QBO signal is apparent at 30 km.

Primrose Lake, Canada (55°N)

Temperature trends from 1973–1985 at Primrose Lake are shown in Figure 6.26. The regression analysis, however, indicates downward as well as upward trends at the different altitudes. These varying trends may be a result of the large interannual variability in high latitudes combined with the missing data. For example, at 30 km, the trend is indicated as 1.5K per decade, while at 35 km it appears to be upward at a rate of 2.5K per decade. Essentially, the trends calculated for the Primrose Lake temperature data may be inconclusive because of the aforementioned large interannual variability and missing monthly average data.

The six rocketsonde sites show downward temperature trends in the stratosphere when the 1969, 1970, and 1971 data are included in the trend analysis. Since rocketsonde sites are uniquely located and few in number, it is impossible to determine a zonal or global trend from these data. There is still disagreement between researchers over differences in the rocketsonde data during the 1970–1972 period.

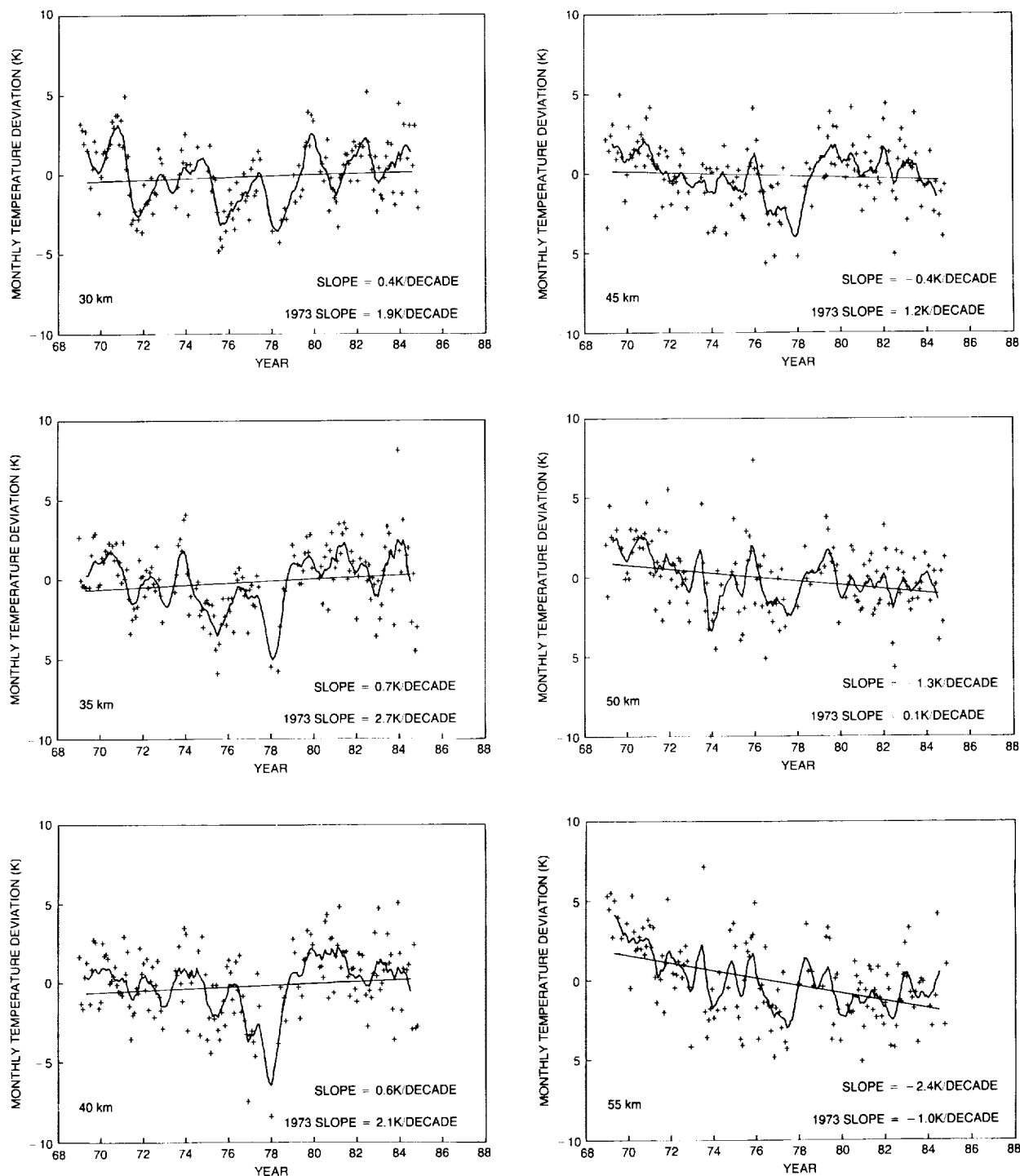## ASCENSION ISLAND 9S 14W

Figure 6.21 Rocket observations for 30–55 km region at Ascension Island. Solid line is smoothed data set (see text). Straight line is 1969–end trend. Crosses denote deviations from monthly mean. First slope is 1969–end of data set trends, second slope is 1973–end of data set trend.
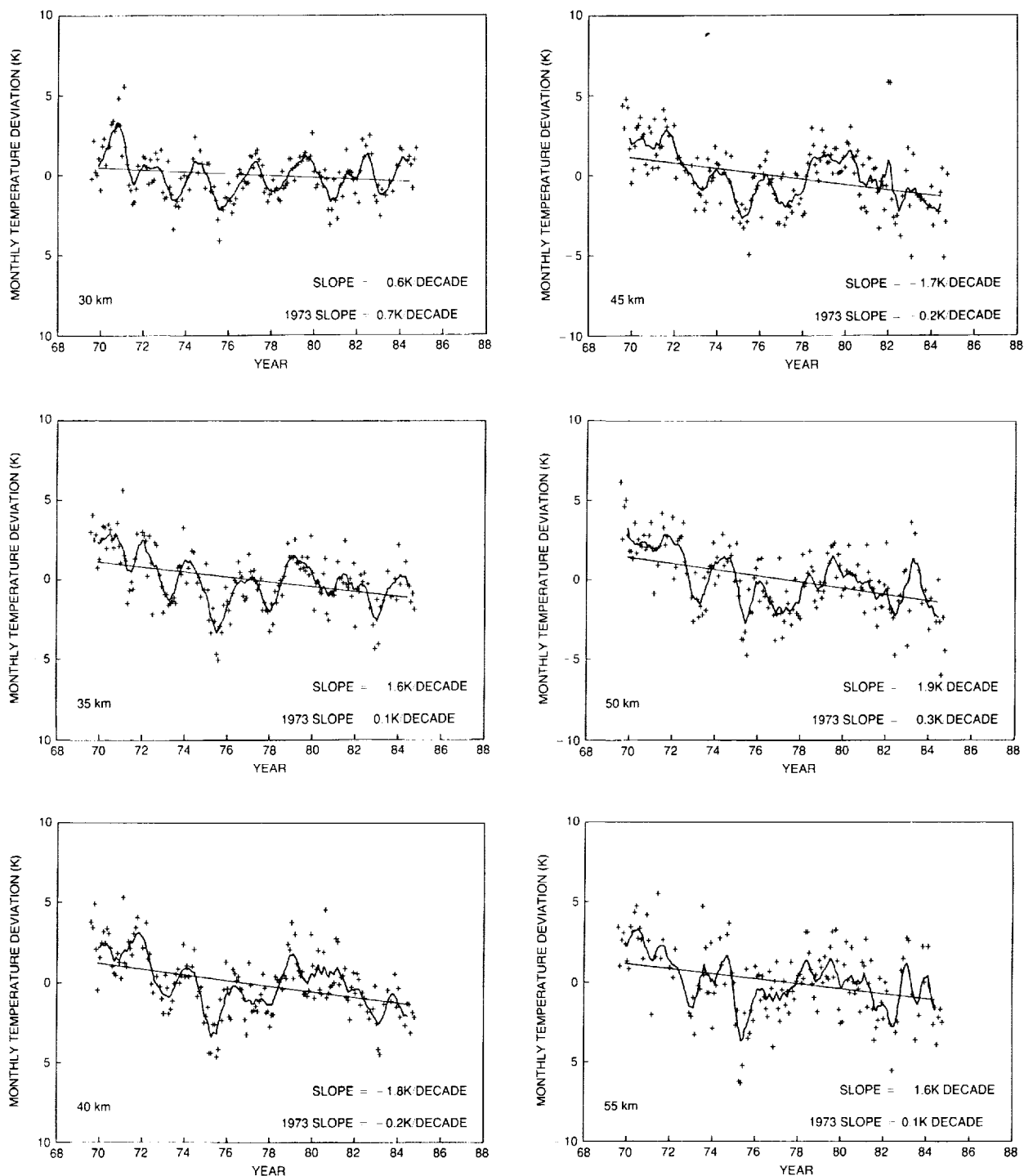
KWAJALEIN ISLAND 9N 168E

Figure 6.22 Same as 6.21 except for Kwajalein.

BARKING SANDS, 22N 160W

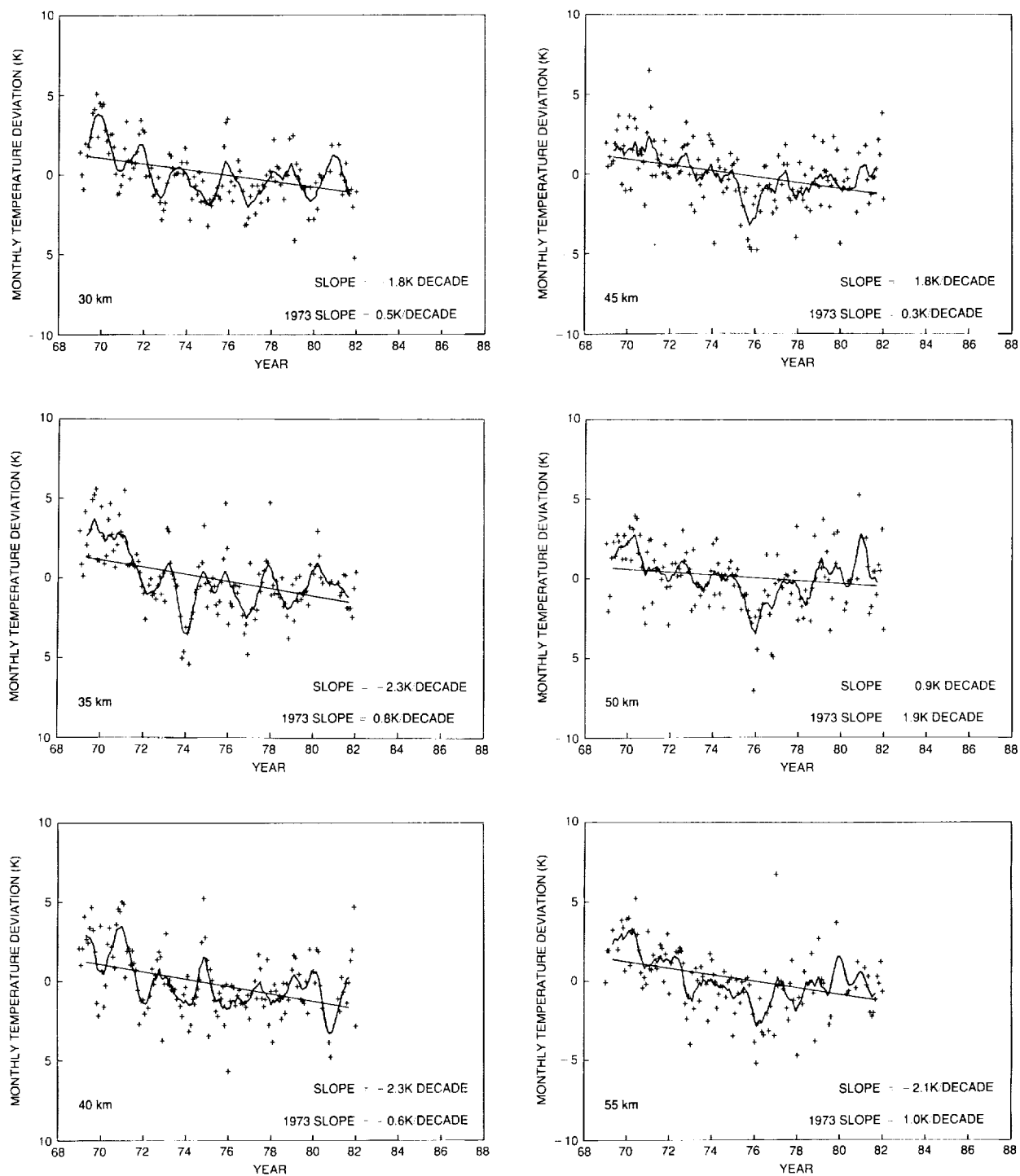**Figure 6.23** Same as 6.21 except for Barking Sands.

CAPE CANAVERAL 28N 81W

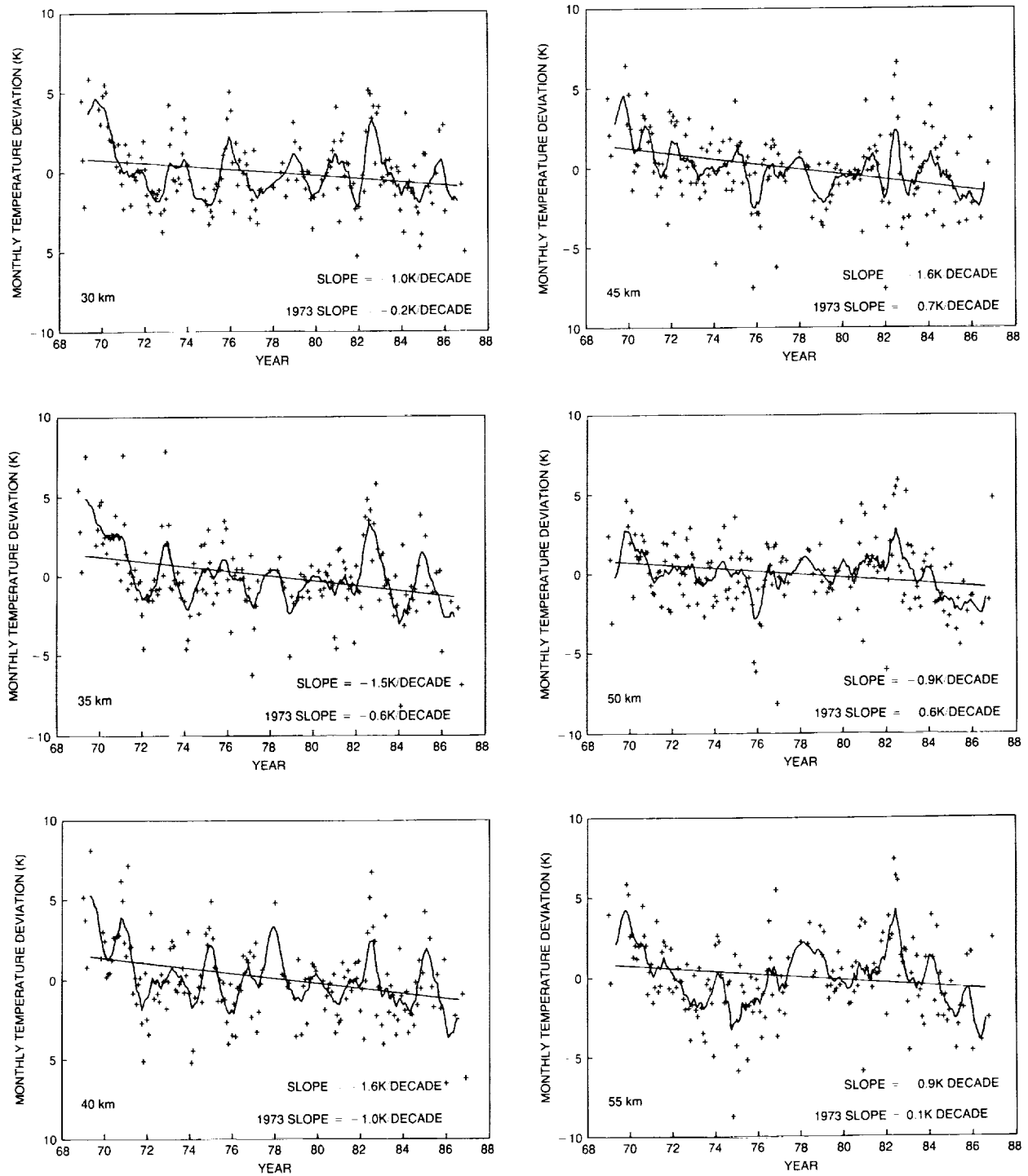**Figure 6.24** Same as 6.21 except for Cape Canaveral.

PT. MUGU 34N 119W

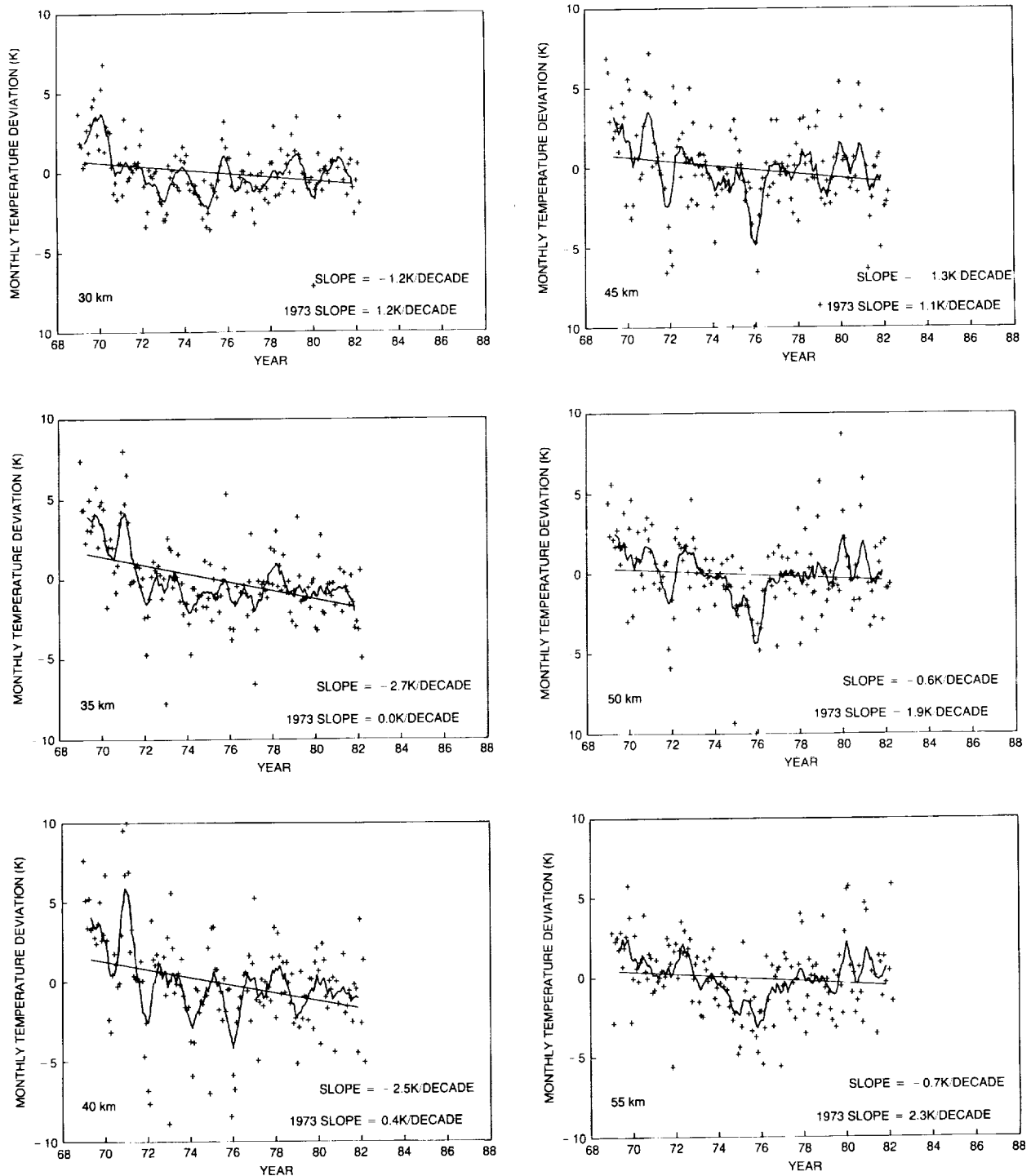**Figure 6.25** Same as 6.21 except for Pt. Mugu.
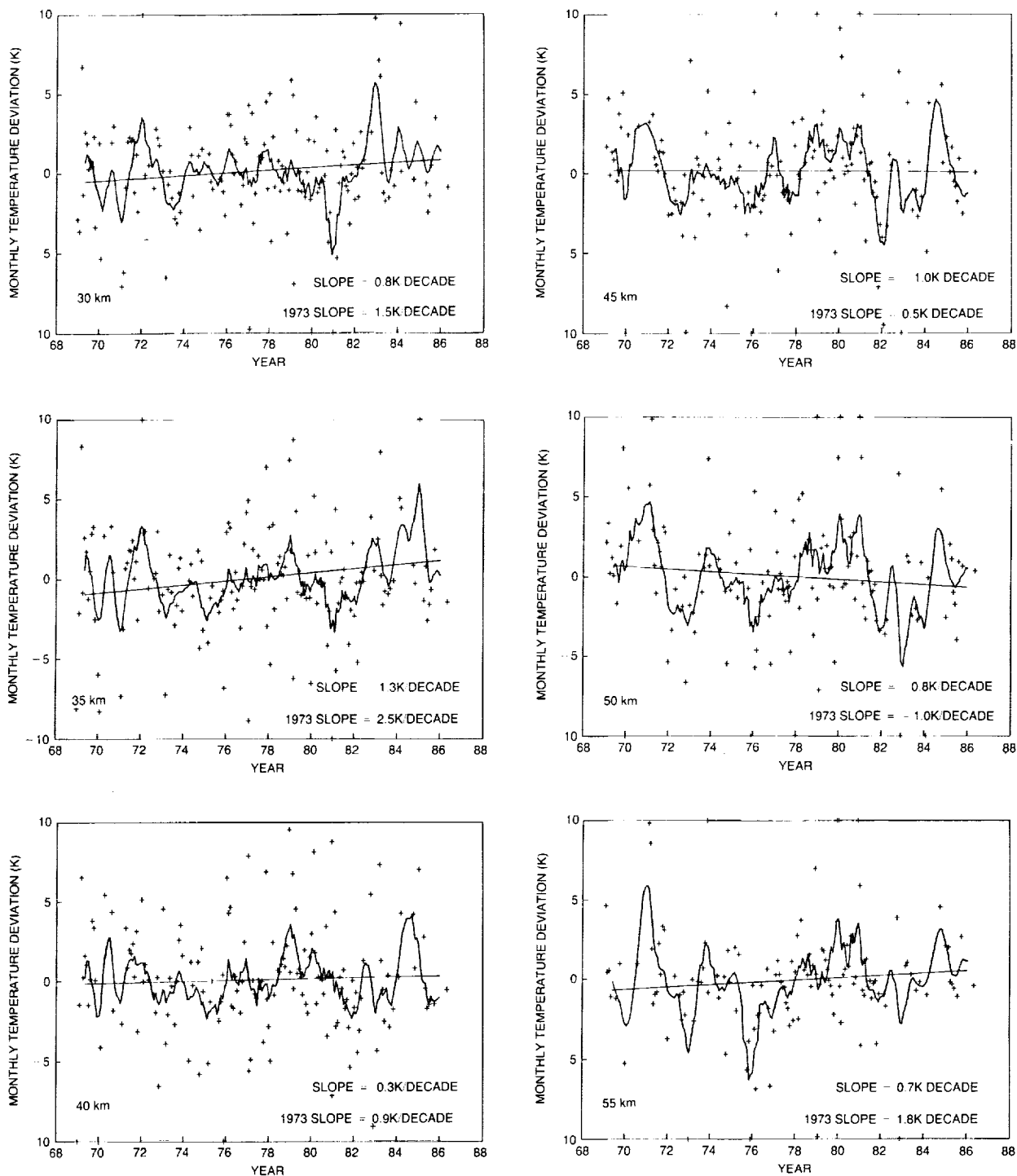
PRIMROSE LAKE 55N 110W

Figure 6.26 Same as 6.21 except for Primrose Lake.

6.4 MECHANISMS FOR ATMOSPHERIC TEMPERATURE TRENDS

In this section, the processes that could drive stratospheric temperature changes are discussed. Over the last 10 years during which satellite measurements have been available, the solar flux, the level of aerosol loading, and the concentrations of trace gases all have changed. Dynamical processes may also contribute to temperature changes. This section outlines the changes in temperature expected from these effects. If most of the processes contributing to the observed stratospheric temperature trends of the last decade can be quantitatively assessed, then it may be possible to infer the reliability of reported ozone changes (e.g., SBUV, SAGE, etc.), as well as model-computed ozone changes.

6.4.1 Global Ozone Changes

In this section, calculations that estimate temperature changes that would result from the global changes in ozone reported by the SBUV and SAGE data processing teams are summarized.

SBUV ozone-mixing ratios have been reported to be declining since 1979, with a maximum decrease of 20 percent at 1 mb from 1979 to 1986. Radiative equilibrium temperature calculations were made using 1979 and 1986 zonal mean SBUV ozone-mixing ratio profiles, at 80°N in June and 0° in March. These two cases were chosen because they represent situations in which dynamical effects should be minimal (Geller et al., 1983). Thus radiative equilibrium temperature computations may provide a reasonable assessment of temperature trends. Figure 6.27 shows SBUV ozone fractional decreases between 1979 and 1986.

The calculations are performed using three different radiative transfer models, as shown in Table 6.11. In Models 1 and 2, the tropospheric water vapor profiles are taken from the McClatchey (McClatchey et al., 1971) tropical and subarctic reference atmospheres for the equatorial and the polar calculations, respectively. Stratospheric water vapor is fixed at 5 ppmv, and the ground temperature is set equal to the air surface temperature. Model 3 has a simplified troposphere and specifies infrared fluxes and tropospheric albedos based on mean values that give approximately the correct upwelling flux at 100 mb. For the tropical equinox calculation, the solar declination angle is fixed at 0°, while for the summer polar calculation, the declination is fixed at 23.5. The surface albedo is set to 0.7 for the polar case and 0.07 for the tropical case, and no clouds are included. The temperatures are time-marched to radiative equilibrium using diurnally averaged solar heating.

Figure 6.28 shows the radiative equilibrium temperature changes resulting from the 1979 to 1986 SBUV ozone changes for the June polar case; Figure 6.29 shows the changes for the March equatorial case. The models are in remarkably close agreement. A maximum temperature decrease of 6.7–7.2K at about 0.5 mb occurs for the June polar case, while a decrease of 5.2–5.5K at 0.5 mb occurs for the March equatorial case. For both cases, the region of maximum cooling is fairly narrow, falling to zero by 2 mb. A temperature difference this sharply peaked may be difficult for satellites having broad instrument weighting functions (see Figure 6.2) to detect. When these temperature changes are convolved with the synthesized SSU–47X weighting function centered at 0.5 mb, the temperature changes that are predicted to be observed by satellite are reduced to -4.8K for the June polar and -3.8K for the March equatorial cases. The 2-year averaged SSU–47X differences (i.e., the 1985 through 1986 data differenced with the 1979 through 1980 data) shown in Table 6.10 show a global change of -1.75K, while SSU–36X (shown in Table 6.9) shows a global change of -1.4K.

Figure 6.27 Fractional decrease between 1979 and 1986 SBUV zonal mean monthly mean ozone mixing ratios. The solid curve is for 80°N in June, and the dashed curve is for 0° at the Equator in March. Units are ppmv.

Table 6.11 Radiative Transfer Models Used in this Section

Model	Organization	Reference
1	NASA/GSFC	Rosenfield et al. (1988)
2	NOAA/GFDL	Schwarzkopf and Fels (1985), Fels and Schwarzkopf (1975), Lacis and Hansen (1974)
3	Univ. of Oxford	Shine (1987)

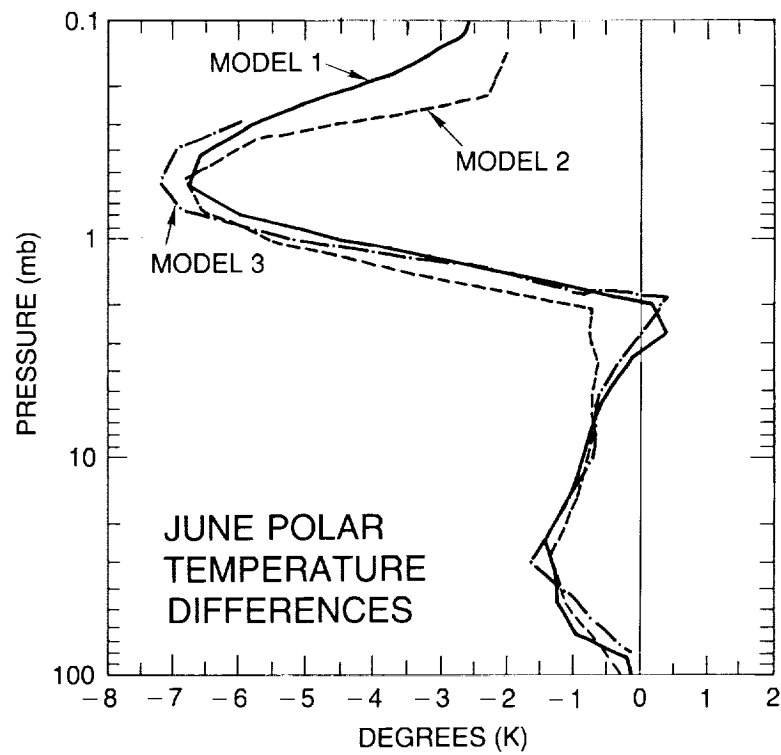**Figure 6.28** Radiative equilibrium temperature differences computed by the three models for the June summer polar case. The differences plotted are computed using 1986 and 1979 ozone data,
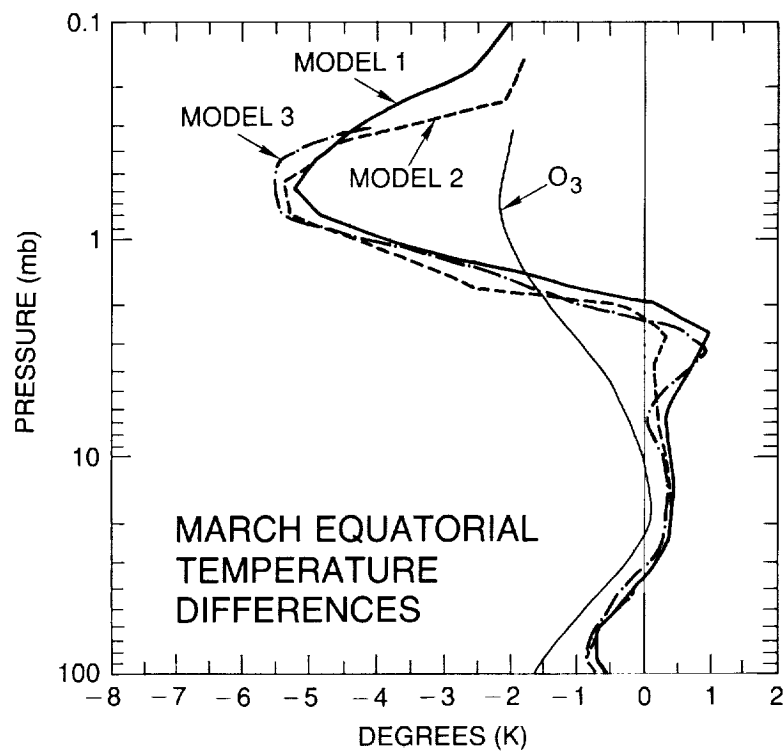

Figure 6.29 As in Figure 6.28 except for the March equatorial case.

The radiative temperature changes expected on the basis of the changes in ozone measured by the SAGE–I and SAGE–II instruments, which give an independent estimate for the period between 1980 and 1986 (cf. Chapter 5), are considered below. The SAGE data used are zonal mean profiles for a latitude band 15°S to 15°N and represent annual averages constructed from seven periods, during which both SAGE–I and SAGE–II sampled the Equator within roughly the same 30-day period of the year. It is important to realize that SAGE measures ozone only between 26 and 50 km. Because the predicted temperature is sensitive to the ozone change above 50 km, two cases have been considered: no ozone change outside 26 to 50 km, and − 5 percent ozone change above 50 km and − 2 percent below 26 km.

Figure 6.30 shows the ozone profiles, and the solar heating and radiatively induced temperature changes computed from Model 2 for the two cases. Notice that, at 47 km, both cases predict changes of about 1K, but above 50 km, the two cases disagree. It remains true, however, that both scenarios yield temperature changes much smaller than those predicted using the SBUV ozone discussed above.

When convolved with the appropriate SSU weighting functions 47X and 36X, the satellite-measured temperature changes are calculated to be:

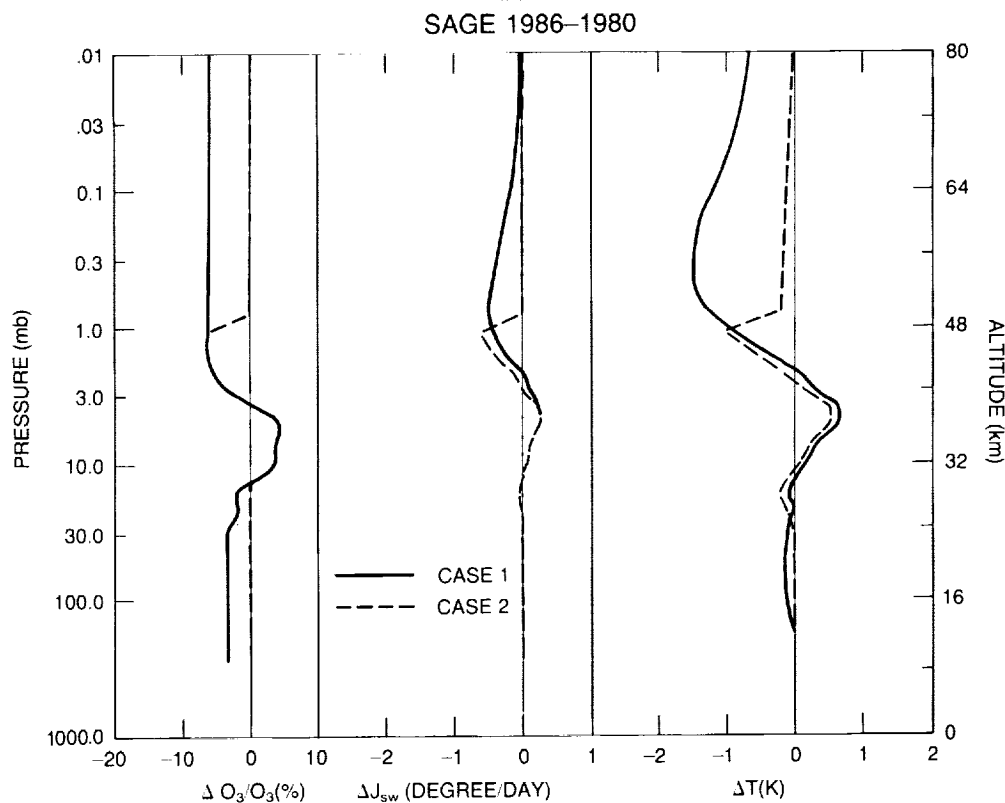| SSU Channels	SAGE Case (a)	SAGE Case (b)	SBUV
47X	− 0.4	− 1.2	− 3.6
36X	− 0.2	− 0.3	− 1.8

Figure 6.30   Radiative equilibrium computation for SAGE-observed ozone.

6.4.2 The Radiative Impact of Other Trace Gases

Significant changes are occurring in the middle atmosphere concentration of other radiatively active gases such as CO_2, CH_4, and N_2O. In the upper stratosphere, a near radiative balance exists between solar radiation absorbed by ozone and infrared radiation emitted by carbon dioxide, ozone, water vapor, and other trace gases. Higher levels of stratospheric trace gases increase infrared emittance and will produce a decrease in temperature. Fels (private communication, 1987) has computed that the increased cooling caused by CO_2 alone to yield a -0.2 to -0.3K change in temperature at 2 mb and a -0.15K change at 10 mb between 1979 and 1986. It is not likely that the expected changes in trace gases other than ozone could significantly modify the upper stratosphere temperature.

6.4.3 Solar Cycle

The solar UV flux that affects the 30 to 70 km region lies between wavelengths of 200 and 300 nm, where the Hartley absorption bands of ozone are located (see WMO, 1986). The radiation absorbed by ozone at these wavelengths gives rise to a strong heating, with a peak at 50 km.

During the course of the solar cycle from its maximum to its minimum, the incident UV flux at the top of the atmosphere decreases. This implies a decrease in the stratospheric heating rates, provided the ozone amounts remain unchanged (an assumption made throughout this section). The change in the UV flux (200 to 300 nm) is not uniform. While the flux at 205 nm changes by about 9 percent, that at 270 nm changes by about 1 percent. A one-dimensional radiative transfer model (Ramaswamy and Kiehl, 1985) is used to investigate the effects of the change in the Hartley band flux at the top of the atmosphere upon the heating rates during solar maximum and solar minimum. The wavelength-dependent reduction applied is based on the results of Heath and Schlesinger (1986) (see also Chapter 7). The resulting changes in the tropical stratospheric heating rates (Figure 6.31) are expressed as the difference between the values at the time of
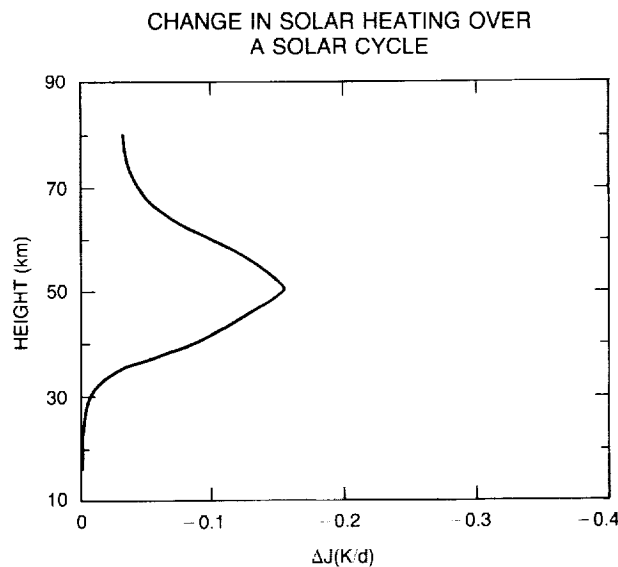

CHANGE IN SOLAR HEATING OVER
A SOLAR CYCLE

Figure 6.31 Changes in solar heating rates due to variations in the ultraviolet flux between solar minimum and solar maximum based on Heath and Schlesinger (1986) and Chapter 7 of this report. Units are degrees Kelvin per day.

CHANGE IN R-C E
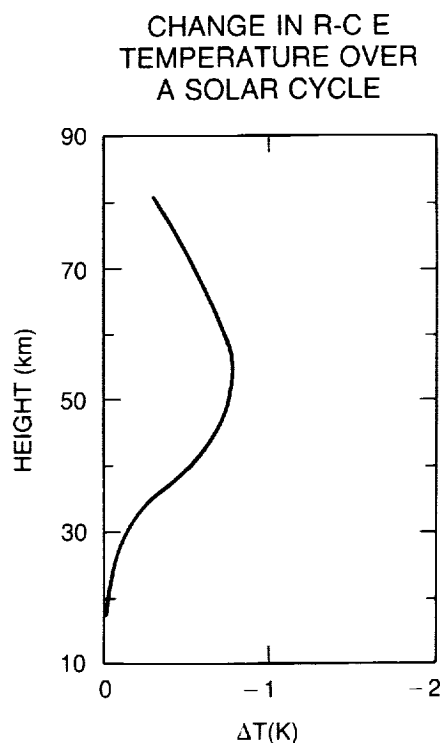TEMPERATURE OVER
A SOLAR CYCLE

Figure 6.32 Changes in radiative–convective equilibrium temperature due to changes in the solar ultraviolet flux over a solar cycle.

solar minimum and those during the solar maximum. The maximum change, about 0.15K per day, occurs where the absolute values are peaked (50 km).

These heating perturbations are treated as a driving force in a radiative–convective equilibrium model (Fels et al., 1980) to investigate the resulting changes in the temperature structure (ozone amount is held fixed). As shown by the results in Figure 6.32, the profile of the temperature perturbations is similar to the profile of the heating rate perturbations. The change in the temperature between the solar minimum and the solar maximum at 50 km in the present calculation is about 0.8K.

6.4.4 Aerosols

Stratospheric aerosol loadings caused by volcanic emissions possess the potential to alter the transfer of radiation and perturb the energy balance of both the troposphere and the stratosphere. Radiative–convective model studies (Pollack et al., 1976; Hansen et al., 1978) have shown that the principal radiative effects of volcanic aerosols (composed typically of ash and sulfuric acid) are to reduce the solar flux in the troposphere and to cause a warming in the lower stratosphere. Part of this warming is a result of aerosol absorption in the solar spectrum, while the other part is caused by absorption of the longwave flux from the troposphere and the subsequent reemission at the colder stratospheric temperatures. As an example of the possible magnitude of this warming, Pollack and Ackerman (1983) estimate an increase in temperature of about 3.5K at 30 mb in the northern tropics due to the El Chichón volcanic cloud.

The magnitude of the warming in the lower stratosphere that results from volcanic emissions depends on the aerosol optical properties, their sizes, and the upwelling longwave flux from the

troposphere, all of which exhibit considerable spatial and temporal variations. The nature of these dependencies is illustrated here for a diurnally averaged tropical atmospheric profile, using a one-dimensional radiative transfer and a radiative–convective model (Ramaswamy and Kiehl, 1985). For the purposes of the present sensitivity study, the aerosols are assumed to have a lognormal size distribution, with a constant number concentration between 16 and 25 km; it may be noted that this was a typical altitude for the El Chichón debris. The optical depth at a wavelength of 0.5 microns is assumed to be 0.08, unless stated otherwise.

The effects of the optical property and the size of the particulates are examined by considering three different cases: 1) a unimodal size distribution (mode radius of 0.08 micron) composed of spherical sulfate drops (optical properties from Palmer and Williams, 1975), 2) a bimodal distribution (two mode radii, 0.02 and 0.2 micron) containing larger particles, characteristic of the El Chichón debris at some locations, and 3) unimodal distribution of dust particles with the same size characteristics as in (1), but with different optical properties (Shettle and Fenn, 1979). The difference between (1) and (2) is due to the size distribution, while the difference between (1) and (3) is due to the optical properties.

The initial perturbations in the solar heating rates for each of the three cases are shown in Figure 6.33a; the perturbations in the longwave heating are shown in Figure 6.33b. Since sulfates absorb only in the near infrared, while dust absorption extends over the entire solar spectrum, the dust-induced solar heating exceeds that caused by the sulfates for similarly sized particles; the sulfates, however, are stronger absorbers than dust in the longwave spectrum. Larger sulfate particles result in increased longwave heating rates. The temperature perturbations are shown in Figure 6.33c. The vertical profile of the changes in the temperature is,

CHANGES IN HEATING RATES AND TEMPERATURE
DUE TO STRATOSPHERIC AEROSOLS

——————— UNIMODAL (SMALL SIZE) SULFATE AEROSOL
– – – – BIMODAL (SMALL & LARGE SIZE) SULFATE AEROSOL
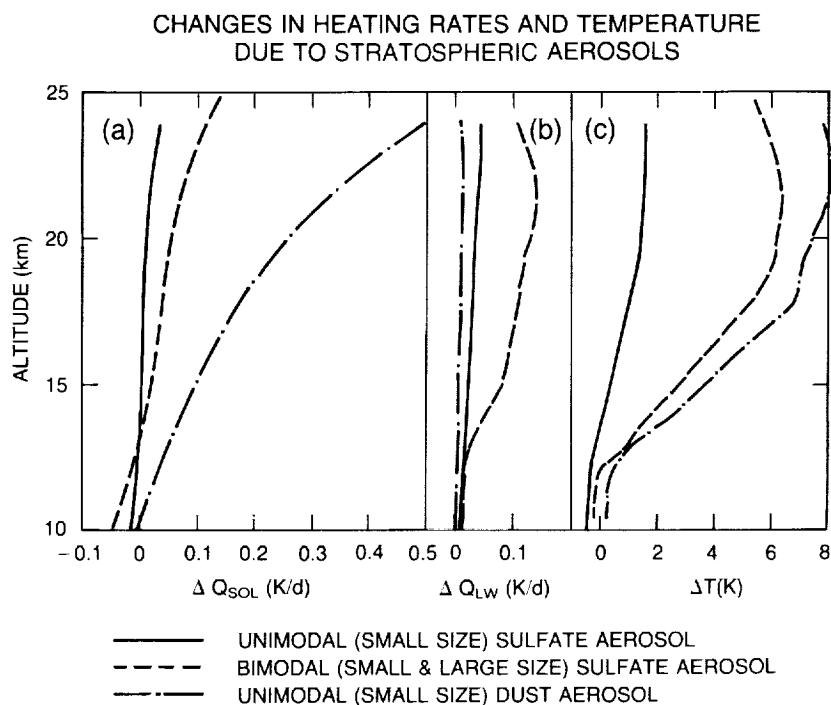—— · —— UNIMODAL (SMALL SIZE) DUST AEROSOL

Figure 6.33 Effect of aerosols with an optical depth of 0.08 on a) the solar heating rate, b) the infrared heating rate, and c) the temperature, for a tropical profile. The solid curve is unimodal sulfate, the dashed curve bimodal sulfate, and the dot–dashed curve unimodal dust aerosol.

in each case, due to the influence of the net (solar and longwave) heating. Thus, the 8K change at 23 km for dust is primarily a consequence of the shortwave absorption, the change of 6K for the bimodal sulfate distribution is due to both solar and longwave perturbations, and the changes for the unimodal sulfate distribution are mostly a result of the longwave heating.

For typical volcanic injections (optical depths 0.1 to 0.3; Toon and Pollack, 1976), the stratospheric heating perturbations increase almost linearly with optical depth (Figure 6.34). The corresponding changes in the radiative–convective equilibrium temperature are shown in Figure 6.35. At 23 km, for example, the temperature perturbation can attain a value of 4K.

To examine the importance of the upwelling longwave flux from the troposphere for the lower stratospheric temperature perturbations, four numerical experiments are considered that involve the unimodal sulfate aerosols and upper tropospheric clouds (cloud stop altitude of 13 km). The aerosol optical depth in each case is assumed to be 0.2. All conditions remain the same unless otherwise specified below. In case 1, a clear sky is assumed. In case 2, nominal values for cloud properties (high cloud emissivity is 0.5) are assumed (Ramaswamy and Ramanathan, 1989); this is similar to the value for an optical depth of 0.2 in Figures 6.34–35. Cases 3 and 4 involve completely cloud-covered troposphere, with case 4 having a high cloud emissivity of 1. Cases 1–4 represent situations in which, successively, less of the upwelling longwave flux is available for absorption by the aerosol particles. Thus, the resulting temperature perturbation at 23 km (listed in Table 6.12) is greatest when this upwelling flux is at its maximum (Case 1; 3.5K), and least when the upwelling flux is at its minimum (Case 4; 1K).
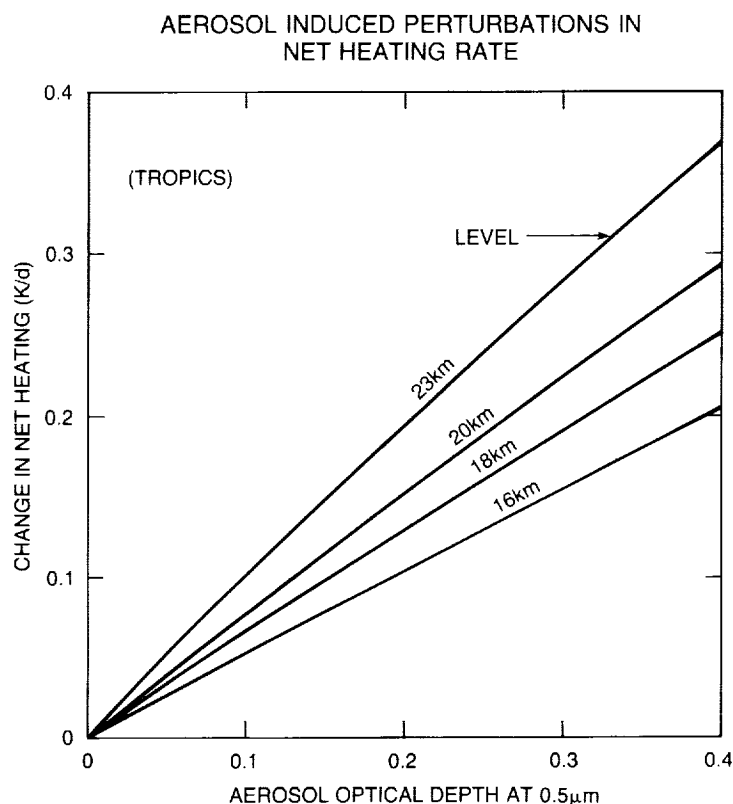

Figure 6.34   Changes in the net heating rate as a function of unimodal sulfate aerosol optical depth in a tropical atmosphere.

AEROSOL INDUCED PERTURBATIONS IN
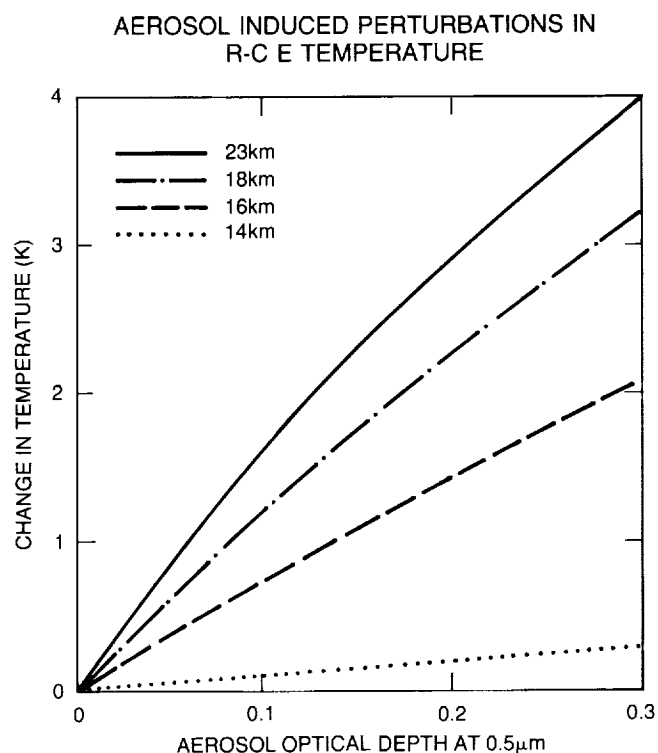R-C E TEMPERATURE

Figure 6.35 Aerosol-induced perturbations in radiative–convective equilibrium temperature as a function of unimodal sulfate aerosol optical depth.

It is tempting at this stage to associate the 1982 temperature deviation from the mean (shown in Section 6.3) with the El Chichón eruption. Pitari et al. (1987) have used a two-dimensional residual circulation model to consider the effects of the El Chichón eruption on temperatures and zonal circulation. Using observed aerosol properties, they estimated a 2–3K temperature increase in the tropical and midlatitudinal lower stratosphere, with negligible changes in the residual circulation. It can be concluded from the one- and two-dimensional model studies that, while a part of the deviation in the observed temperatures can be attributed to the volcanic emission, the issue cannot be resolved unambiguously because of uncertainties concerning the

Table 6.12 Dependence of Radiative Convective Equilibrium Temperatures on Cloud Properties

Aerosols Between 16 and 25 km
Low cloud (top 3.0 km; cloud cover = 0.31)
Middle cloud (top 5.6 km; cloud cover = 0.09)
    (low and middle clouds assumed black)
High cloud (top 10.4 kms)

Experiment Description	Change in Temperature $[\delta\ T\ (K)]$ (23 km)
1. Clear	3.5
2. Nominal Clouds (High cloud cover = 0.23, Emissivity = 0.5)	2.8
3. Same as 2 except high cloud cover = 1.0	1.5
4. Same as 3 except emissivity of high cloud = 1.0	1.0

spatial and temporal variations in the aerosol optical properties. The problem of radiatively active species interacting simultaneously with the microphysical and large-scale dynamical processes must be addressed comprehensively before a definitive answer can be obtained from the models. Further, observations of both aerosol properties and temperatures also need to be accurate, since the lower stratosphere has a large radiative time constant.

6.4.5 Dynamics

The global circulation of the stratosphere is established largely through the interplay between the external tropospheric forcing and the radiative heating and cooling within the stratosphere. It has long been realized that trends in both temperature and ozone can result, in principle, from dynamical trends in the stratosphere. These changes can result from an alteration in the level of wave activity through tropospheric forcing or through changes in the wave propagation characteristics of the stratosphere itself. The latter changes can result from changes in winds and temperatures through a variation in the concentration of radiatively active gases, aerosols, or the solar flux. Since the concentrations of the radiatively active gases are, in turn, influenced by the transport properties of the stratosphere, which are partially determined by dynamical forcing, all of these processes are interdependent.

Eddy activity in the stratosphere tends to force the stratosphere away from a state of near-radiative equilibrium. In the absence of dynamical activity, long-wave cooling would balance short-wave heating everywhere except for small departures caused by thermal inertia and the seasonal cycle. Therefore, trends in both stratospheric temperatures and trace gases cannot be considered independent processes.

A number of authors have considered the feedbacks that might result from ozone depletions or solar cycle changes altering the insolation, the large-scale winter jet structure, and ultimately the propagation properties of large-scale waves (Schoeberl and Strobel, 1978; Fels et al., 1980; Callis et al., 1985b; Kiehl and Boville, 1988). These studies, which fixed the troposphere, found no significant change in the stratospheric dynamical activity except for scenarios of very sizable (>50 percent) ozone depletions. For example, using perpetual conditions from January, Kiehl and Boville (1988) concluded that the dynamical response to halving ozone uniformly was small. The dynamical response to a realistic ozone reduction scenario, with the largest ozone changes confined to high latitudes, was found to be not only quite different to that for uniform ozone reductions, but even smaller.

An estimate of the tropical stratopause temperature change caused by altered dynamics may be obtained by assuming that the globally averaged stratosphere at any level is in radiative equilibrium. If it is assumed that the largest temperature changes are likely to be in the polar night, and that these are, at most, on the order of 30K (Hamilton, 1982), then compensating changes on the order of several degrees in the tropics would be expected. This estimate is confirmed by Hamilton's analysis, which shows that even in years whose polar stratopause temperatures differ by 30K, the tropical temperatures at 1 mb are the same to within a few degrees. Thus, any dynamical process in the tropics cannot realistically be expected to mask the long-term temperature changes that would result from the SBUV-reported ozone changes in the upper stratosphere.

It is more difficult to assess how changes in the tropospheric forcing of the stratosphere might alter the lower stratospheric temperature structure. Current three-dimensional model simulations have difficulty even reproducing the observed stratosphere (Mahlman and Umscheid,

1984), although substantial improvements have been made by increasing the model resolution (Mahlman and Umscheid, 1987). A possible reason for a change in the tropospheric forcing is a change in the locations and intensity of convective regions. These regions can change in response to alterations in the fluxes of sensible and latent heat that result from a change in surface properties. While large-scale modification of the land surface has the potential to produce significant changes in the surface fluxes, a more likely candidate is a change in the distributions of sea surface temperatures and sea ice (e.g., Austin, private communication, 1987).

The sea surface temperature distribution is not independent of the atmospheric circulation. The major ocean current systems are primarily wind driven, so that the sea surface temperature distribution is intimately coupled with the atmospheric circulation on time scales ranging upwards from about a month. This coupling of atmosphere and ocean has the potential to introduce oscillations with time scales of years to millennia, which makes the definition and identification of truly external forcing processes difficult. An example of a fluctuation of the coupled ocean–atmosphere system is the El Niño–Southern Oscillation (ENSO), which has received a great deal of attention in recent years. Changes in the surface temperatures of the tropical Pacific Ocean have been shown to introduce changes in tropical convection and in planetary wave patterns in the extratropics of the Northern Hemisphere (see, e.g., Blackmon et al., 1983). There appears to be little doubt that variations in the tropical Pacific surface temperatures are a manifestation of the coupling with the atmosphere, and even though a considerable amount of work has been done on modeling the tropospheric response to sea surface temperatures, little information is available on the stratospheric response.

Figure 6.6 shows the long-term fluctuations in temperatures in the 30 to 100 mb layer at north temperature latitude. The amplitude of these fluctuations was less than 1K over decadal periods; since the source of these changes has not been identified radiatively, it can be hypothesized that they are dynamical in origin. Thus, a crude estimate of the magnitude of dynamical contributions to trends could be 1K per decade in the lower stratosphere.

Long-term changes in tropospheric dynamical activity could certainly produce midlatitude and polar stratospheric temperature trends as large as the observed year-to-year changes, and perhaps larger. These changes are as large as the predicted changes because of trends in the radiative source gases discussed earlier; therefore, they will add to the uncertainty in identifying trend mechanisms from temperature observations alone. However, tropical stratospheric responses to midlatitude dynamical changes are expected to be quite small, so that unambiguous trend detection may be possible in that region.

6.4.6 Radiative Photochemical Models

Radiative photochemical models predict a variation in stratospheric ozone and temperature during solar cycles and as the concentrations of ozone-catalyzing minor constituents increase with time (see Chapter 7). The calculation of the expected change in stratospheric temperature is complicated by feedbacks involving ozone photochemistry. For example, a decrease in temperature leads to some increase in ozone, which acts to offset the original temperature decline.

Table 6.13 summarizes the results from one-dimensional models at the altitude of peak cooling. All models listed are photochemical and include the effects of increased CO_2, CH_4, N_2O, and chlorofluorocarbons (and sometimes NO_x). The resultant decreases in ozone are also incorporated. The calculations are grouped into sets covering approximately the same period, and the trend in degrees Kelvin per decade is given for comparison. Since the periods shown are

Table 6.13 Comparison of Calculated Cooling From One-Dimensional Radiative–Photochemical Models Near to the Level of Peak Cooling

Paper	Period	Approximate Level of Peak Cooling	Temp Change	Approximate Change in temp/ decade
Brasseur and De Rudder	1960–80	45 km	−3.4K	−1.7K/decade
Bruhl	1960–85	1.5 mb (45 km)	−3.9K	−1.6K/decade
Vupputuri	1960–85	(at 42 km)	−3.8K	−1.5K/decade
Wuebbles	1960–83	42 km	−3.4K	−1.5K/decade
Brasseur and De Rudder	1940–80	45 km	−5.0K	−1.25K/decade
Bruhl	1935–85	1.5 mb (45 km)	−4.9K	−1.0K/decade
Owens et al.	1940–85	46 km	−3.8K	−0.84K/decade
Vupputuri	1940–85	(at 42 km)	−4.5K	−1.0K/decade
Wang et al.	1950–80	48 km	−1.9K	−0.6K/decade
Wuebbles	1950–80	42 km	−3.2K	−1.1K/decade
Bruhl	1860–1985	1.5 mb (45 km)	−6.0K	−0.48K/decade
Vupputuri	1850–1980	44 km	−5.5K	−0.42K/decade

roughly the length of an integral number of solar cycles, models that incorporate solar cycle changes can be compared with those that do not. Most of the model-computed temperature changes in Table 6.13 are caused by changes in the ozone. Bruhl (1987), for example, calculates a peak cooling of 1K between 1960 and 1985 for the CO_2 only, and the CO_2, CH_4, and N_2O only scenarios; this compares with a value of nearly 4K when the chlorofluorocarbons are included.

The agreement between different model calculations is good, particularly for the cooling over the past two or three decades. In the 40 to 50 km layer, these models predict a change of −1.5 to −1.7K over the last decade. The two-dimensional model computations presented in Chapter 7 give similar results.

Table 6.14 shows the cooling calculated at around 30 mb (24 km) for the same sets of calculations. The agreement between calculations is not as good as might be expected near a transition level. Bruhl's model, in particular, calculates a smaller cooling at 30 mb, since the height at which tropospheric warming changes to stratospheric cooling is several kilometers above the transition level found in other models. This level is particularly difficult to calculate and will depend on the particular convective scheme incorporated in the troposphere, as well as on other modeling details, such as vertical resolution. Thus trends estimated at the 30 mb level are likely to be subject to a greater uncertainty than those at lower pressures.

6.5 CONCLUSIONS

The stratospheric satellite, rocket, and radiosonde data sets analyzed in this chapter have been intercompared in detail. Temperature changes from 1979 to 1986 have been determined using radiosondes (Free University of Berlin and Angell and Korshover 1983a) and satellite radiances (United Kingdom Meteorological Office and NMC data). Radiosonde data above 30 mb were not considered reliable for trend determination. The rocket data used here have been edited extensively and improved so that the results are not comparable to previous studies. The rocket data and zonal mean satellite data were intercompared, and trends were determined over the longer rocket data period.

Table 6.14 Comparison of Calculated Cooling From One-Dimensional Radiative–Photochemical Models at About 30 mb (24 km)

Paper	Period	Approximate Level of Peak Cooling	Temp Change	Approximate Change in temp/ decade
Bruhl	1960–85	30 mb (24 km)	almost zero	
Labitzke et al.	1970–80	24 km	−0.2K	−0.2K/decade
Labitzke et al.	1960–85	24 km	−0.6K	−0.24K/decade
Vupputuri	1960–85	25 km	−0.8K	−0.32K/decade
Wuebbles	1960–83	24 km	−0.45K	−0.2K/decade
Owens et al.	1940–85	24 km	−0.6K	−0.13K/decade
Vupputuri	1940–85	25 km	−1.2K	−0.27K/decade
Wang et al.	1950–80	24 km	−0.2K	−0.07K/decade
Wuebbles	1950–83	24 km	−0.47K	−0.14K/decade
Bruhl	1860–1985	30 mb (24 km)	−0.3K	−0.02K/decade
Vupputuri	1850–1980	25 km	−1.6K	−0.12K/decade

This chapter also includes an investigation of the processes that could produce stratospheric temperature trends. These processes include global changes in ozone, solar flux, concentration of other trace constituents, and aerosol loading, as well as dynamical changes. The major conclusions are outlined below:

• The radiosonde and satellite data sets generally intercompare very well, although some periods of disagreement exist. Figure 6.17 shows the computed difference in global temperatures for 1985/86–1979/80. The largest global decline is in the upper stratosphere, with a computed change of −1.75K ±1.0K.

• The rocket data have insufficient spatial coverage to establish global trends and are subject to some uncertainties. Longer term trends from rocketsondes starting in 1969 indicate a cooling on the order of −1 to −2K per decade in the mid- to upper stratosphere. However, if the trends are calculated starting in 1973, they range from −1K per decade up to 2K per decade (warming). Hence, rocketsonde trends are subject to large uncertainties.

• Long-term trends in the lower stratosphere derived from radiosonde-based data sets show no significant cooling except in the Tropics and over Antarctica.

• There is a warming of the lower and middle stratosphere in the 1982–1983 period, which appears to be associated with, and is consistent with, radiative heating of the El Chichón aerosol cloud.

• Standard interactive photochemical and radiative transfer models estimate a cooling of the upper stratosphere of −1.2 to −1.7K per decade for 1970–1990 because of the ozone and trace gas changes. Since 1979, an additional cooling of −0.8K has occurred due to a decrease in the solar flux as part of the solar cycle.

• Using the reported SBUV ozone changes from 1979 to 1986, a radiative equilibrium tropical temperature decline of 5.5K can be computed. An additional 0.8K decline is expected as a result of the decrease in solar flux over that phase of the solar cycle. When this change is convolved with the SSU 47X weighting function centered at 0.5 mb, the detectable temperature change is -4.6K. This compares to the observed -1.3K ± 1K tropical change (Figure 6.18). Thus, the reported SBUV ozone changes in the upper stratosphere appear to be inconsistent with the observed temperature changes, while SAGE-reported ozone changes are not.